BEYOND LINE-OF-SIGHT

CONFERENCE

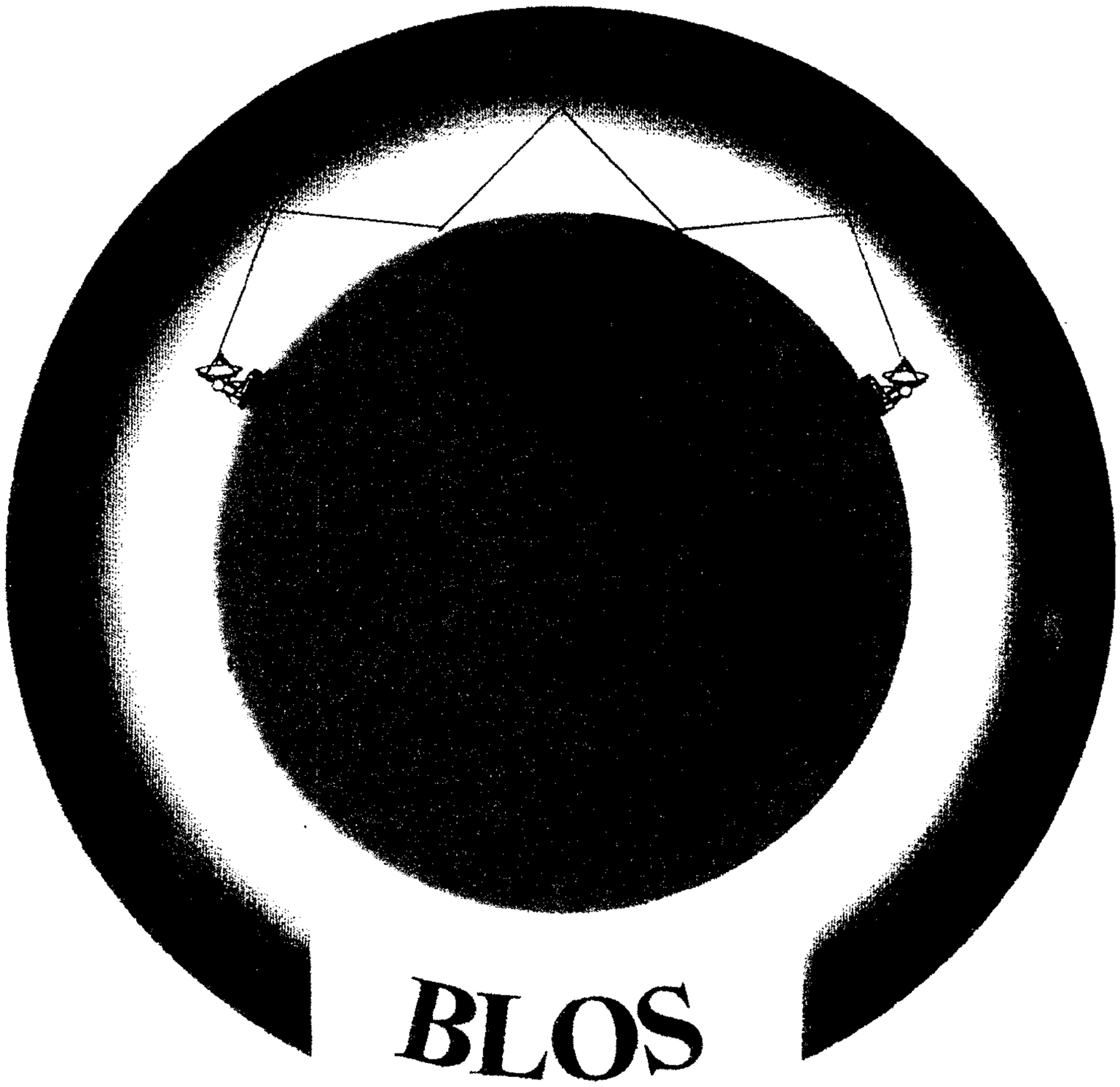

BLOS

2 - 4 AUGUST 1994
AUSTIN, TEXAS

HOSTED BY
APPLIED RESEARCH LABORATORIES
THE UNIVERSITY OF TEXAS AT AUSTIN

REFRACTIVE PROPAGATION EFFECTS MEASURED BY LIDAR

C. R. Philbrick and D. W. Blood
Applied Research Laboratory/Penn State University
P.O. Box 30, State College, PA 16804
(814) 863-8243, Fax (814) 863-8783

ABSTRACT

A multi-wavelength Raman lidar has been developed and used to measure the profiles of water vapor, temperature and other atmospheric properties in the troposphere under a wide range of geophysical conditions. The LAMP lidar instrument is transportable and has been used to make measurements at several locations in addition to our local site, including shipboard measurements between Arctic and Antarctic and in a coastal environment at Point Mugu, CA. The Raman technique provides an accurate way to measure the profiles of water vapor from the ratio of the Raman vibrational backscatter signal from water vapor to that of nitrogen. The lidar has been used both to obtain water vapor profiles from molecular Raman vibrational scattering at several wavelengths, and temperature profiles from Raman rotational scattering at 528 and 530 nm. The water vapor measurements have been made using the vibrational Raman backscatter intensity from the 660/607 ratio from the 532 nm, 407/387 ratio from 355 nm, or the 294/283 ratio from 266 nm laser radiation.

Lidar measurements of the atmospheric refractive environment of particular interest were made during 1993 at Point Mugu, CA, including the period of Project VOCAR (Variability of Coastal Atmospheric Refractivity). The data were averaged and used to compute profiles of refractivity, N, and modified refractivity, M, at 75 m resolution in the lower tropospheric region (0 - 5000 m). The lidar data is stored at one minute intervals and the temporal variation of refractive index is typically examined at intervals of 30 minutes. Both the lidar and balloon (radiosonde) tropospheric measurements have been used for analysis of the propagation conditions through the use of the Navy's RPO, IREPS and EREPS PC programs.

INTRODUCTION

The variations of the radar refractive index are due to variations in the density of the scattering medium. The large scattering dipole moment of some species, such as water vapor, produce a relatively larger change in refractive index. Because the water vapor concentration in the lower atmosphere is highly variable, it makes the strongest contribution to the variations of the refractive index. So, the problem becomes one of first, accurately measuring the water vapor with good spatial and temporal resolution, and second, measuring the density profile with enough resolution to observe significant changes. The variations of the N_2 and O_2 molecular profiles, that contribute 97 to 99% of the density in the troposphere, do not exhibit the rapid changes or the strong gradients that we find in the water vapor. We have chosen to make the density measurement from use of the equations of state and measurements of the temperature and a ground based value of pressure. This approach is normally adopted in meteorology as a consequence of the fact that reliable sensors for the temperature measurement exist and hydrostatic equilibrium of the atmosphere can be assumed under most conditions. The equations which are usually adopted for calculation of the refractive index are based upon temperature, pressure and water vapor partial pressure.

Measurement Techniques

During the past twenty years, researchers at several laboratories have demonstrated that lidar has special capabilities for remote sensing of many different properties of the atmosphere. One of the techniques which shows a great deal of promise for several applications is Raman scattering. In this description, our application of the Raman scattering techniques to obtain profiles of water vapor and temperature in the lower atmosphere is presented. The first Raman measurements of atmospheric properties with lidar were carried out in the late 1960's by Leonard (1967) and Cooney (1968). Two years later, Melfi, et al. (1969) and Cooney (1970, 1971) showed that it was possible to measure water

vapor using the Raman lidar technique. A significant contribution was made by Inaba and Kobayasi (1972) in suggesting several species that could potentially be measured using vibrational Raman techniques. While the early tests [Melfi et al. (1969), Cooney (1970, 1971) and Strauch et al. (1972)] showed that it was possible to measure the water vapor with limited range and accuracy, recent investigations have demonstrated significant improvements. Particularly, the investigations of Vaughan et al. (1988), Melfi et al. (1989), and Whiteman et al. (1992) have demonstrated rather convincingly that the Raman technique has a high potential for making accurate water vapor measurements. A most useful review of the Raman and DIAL lidar techniques applied to the water vapor measurement has been prepared by Grant (1991). The measurements of water vapor during the daytime have been demonstrated by Renaut and Capitini (1988) using the solar blind region of the ultraviolet spectrum. Their work indicated that the optimum wavelength for the measurement was near the fourth harmonic for the Nd:YAG laser. At this wavelength, the measurements of N_2 and H_2O are contaminated, at least to a small degree, by the absorption of O_3 and SO_2 in the lower troposphere, however, it appears that an adequate correction can be obtained from the use of the measured Raman signals of the N_2 and O_2 compared to the known mixing ratio.

At tropospheric altitudes, the Raman N_2 profile together with the multi-wavelength backscatter should allow the separation of the extinction, backscatter due to particles and the molecular backscatter signals. The advantage in using the Raman signals in the lower atmosphere is clear from the profiles shown above. Figure 1 shows a representation of the spectral signatures which would be expected from the back-scatter due to the 532 nm laser radiation in an atmospheric volume. The laser is injection seeded to give a line-width of about 80 MHz and thus the particle back-scatter is of that spectral width, while the molecular peaks are broadened by the thermal Doppler velocity spreading. The vibrational Raman scattering peaks are shown for O_2, N_2 and H_2O, and around each of the peaks is also shown the broadening due to the rotational state distribution around each vibrational state. Only the first Stokes vibrational states are indicated, since the simple molecules have large vibrational energy state separation and the anti-Stokes lines are not normally populated. The figure shows the large cross-section differences between the processes involved. The Raman H_2O signal measured as a ratio to the Raman N_2 signal provides a profile which is proportional to the water vapor concentration. The N_2 fraction of the atmospheric profile is known, and the atmospheric profile can be obtained from the temperature profile combined with a surface pressure value. The error caused by the extinction differences between the backscatter wavelengths is small (few percent) and can be corrected using the results from multiple wavelengths.

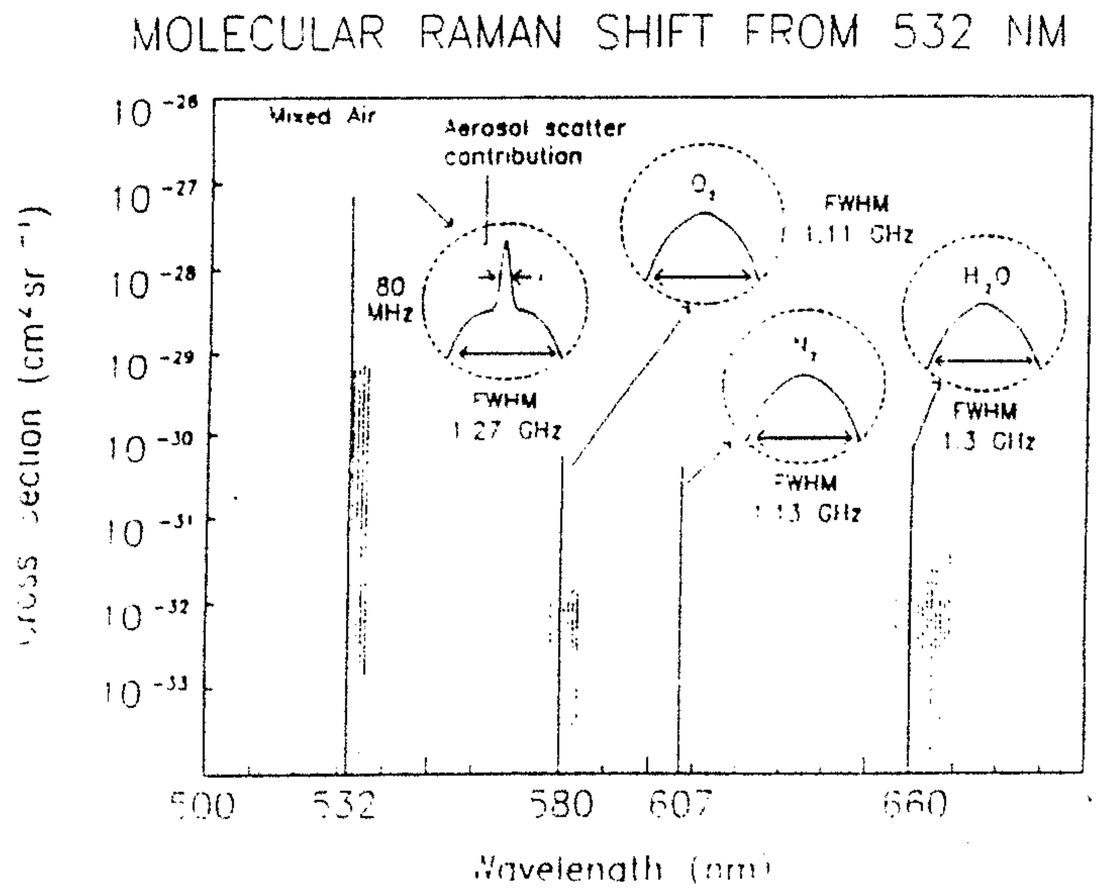

Figure 1. Descriptive representation of the vibrational and rotational Raman signals expected for radiation of an atmospheric volume with 532 nm laser.

While demonstrations by several researchers have shown the potential of lidar to measure many properties of the atmosphere, there have been few efforts to develop the lidar techniques sufficiently for them to be used for routine measurements. The research lidars generally require attentive interaction by highly specialized personnel to obtain useful measurements and thus the investigations have been generally limited to short and intensive measurement periods. The transition of the technical capability of lidar to operational applications in meteorological data collection,

atmospheric physics investigations, studies of the environment, investigations of radiative transport and global climate analysis requires that instrumentation be improved and automated. All of the properties measured by current rawinsonde balloons and meteorological rockets can be measured by lidar remote sensing techniques which have been demonstrated to varying degrees in research laboratories.

The rotational Raman technique for temperature measurements was reported by Cooney (1972). A double grating monochrometer was used by Arshinov, et al. (1983) to measure the rotational Raman spectrum in 1983. Hauchecorne, et al. (1992) and Nedeljkovic, et al. (1993) demonstrated the capability to measure the temperature using narrow-band filter technology in the upper troposphere and lower stratosphere. Figure 2 shows the way that we are using the rotational Raman signal for temperature profile determination. We are making use of the rotational Raman envelop of several lines which pass through a narrow band filter. The molecular species of the atmosphere, principally N_2, O_2 and to some degree H_2O, contribute to the envelop of lines on either side of fundamental laser wavelength. In our case, we measure the lines in the rotational states at the 530 and 528 nm filter bands. The envelop shape is determined by the population of the rotational states under the temperature distribution of the gas in the volume, which is illuminated by the doubled Nd:YAG laser at 532 nm. There are envelops on both the long and short wavelength sides of the fundamental exciting frequency, however we have chosen to work on the short wavelength, higher energy, side of the distribution in case there is any excitation from fluorescent transitions. In Figure 2, the ratio between the intensities of the two filter bands is indicated as a way of directly determining the temperature. While this curve is based upon a calculation, we use a method of comparison of a rawinsonde balloon measurements with the measured results to develop a calibration curve based upon that empirical fit. With the measured temperature profile and a ground based measurement of the surface pressure, the profiles of the structure properties, density, pressure and temperature are all available from the calculations based upon the hydrostatic equation and the ideal gas law. The calculated profile of density can be used to obtain the N_2 profile to place an absolute density of the water vapor from the ratio of vibrational Raman signals.

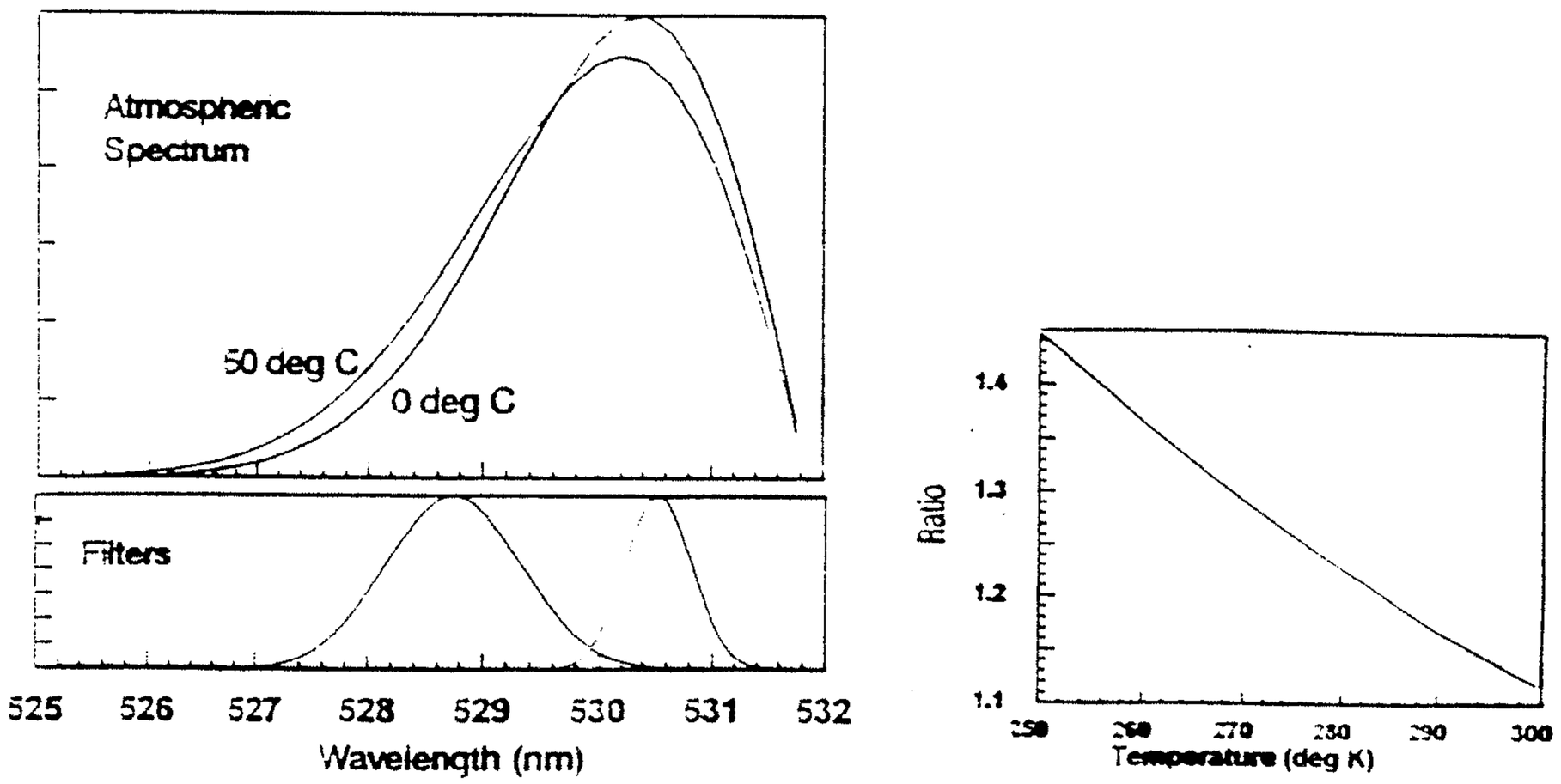

Figure 2. Representation of the use of the rotational Raman spectra for measurements of the temperature profiles in the troposphere.

The first major field experiment using the LAMP lidar was the LADIMAS (LAtitudinal DIstribution of Middle Atmosphere Structure) campaign [Philbrick, et al. (1992, 1994). The results from the LADIMAS experiment [Philbrick, et al. (1992, 1993, 1994a, 1994b), Stevens, et al. (1993, 1994), Croskey (1993), Maruvada (1993), McKinley (1993), Haris (1994)] have provided a unique data set to improve our understanding of the middle atmosphere properties. The project included coordinated ship-board measurements between 70°N to 65°S and measurements at the Andoya rocket range to study the structure, dynamics and chemistry of the atmosphere. Results on dynamical processes, such as gravity waves, as well as, the formation of the layers of meteoric ion and neutral species, have been obtained using lidars, digisonde, microwave radiometer, and spectrometers. The cooperative study

of the atmosphere was undertaken by researchers from several laboratories, including Penn State University, University Bonn, University Wuppertal, Lowell University, and others. Instruments were assembled aboard the German research vessel *RV POLARSTERN* while this vessel was sailing from the Arctic to the Antarctic between October 8, 1991 and January 2, 1992.

The second major field investigation included a set of three measurement periods using the LAMP lidar at NAWC Point Mugu, CA, during the period July-November 1993. This location provided the opportunity to measure the properties of the marine costal environment at a time of concentrated atmospheric measurements associated with a program called VOCAR (Variability of Coastal Atmospheric Refractivity). In addition, the instrument has been used for extensive testing at Penn State University while not involved in these field experiments.

LAMP System Description

The LAMP (Lidar Atmospheric Measurements Program) lidar profiler was placed in service at Penn State University during the Summer of 1991 [Philbrick, et al. (1992)]. The LAMP lidar uses two wavelengths in the upward propagating beam and up to eight detectors in the receiver. The instrument is arranged in a coaxial configuration, which permits useful measurements in the near field, as well as in the far field, see Figure 3. Two detector systems have been prepared for the instrument, one for high altitude measurements and one which is specialized on the low altitude region. The high altitude detector system is used to obtain data between 1 km and 80 km. It uses a mechanical shutter to block the high intensity, low altitude signal, from the two high altitude detectors until the beam has reached an altitude of 18 km. The low altitude detector has the capability of measuring two N_2 and two H_2O vibrational Raman channels simultaneously and measuring two wavelengths of the rotational Raman spectrum for temperature determination. The original high altitude detector was designed to directly attach the telescope by an optical transfer relay, however, the current use of an optical fiber permits the use of either detector.

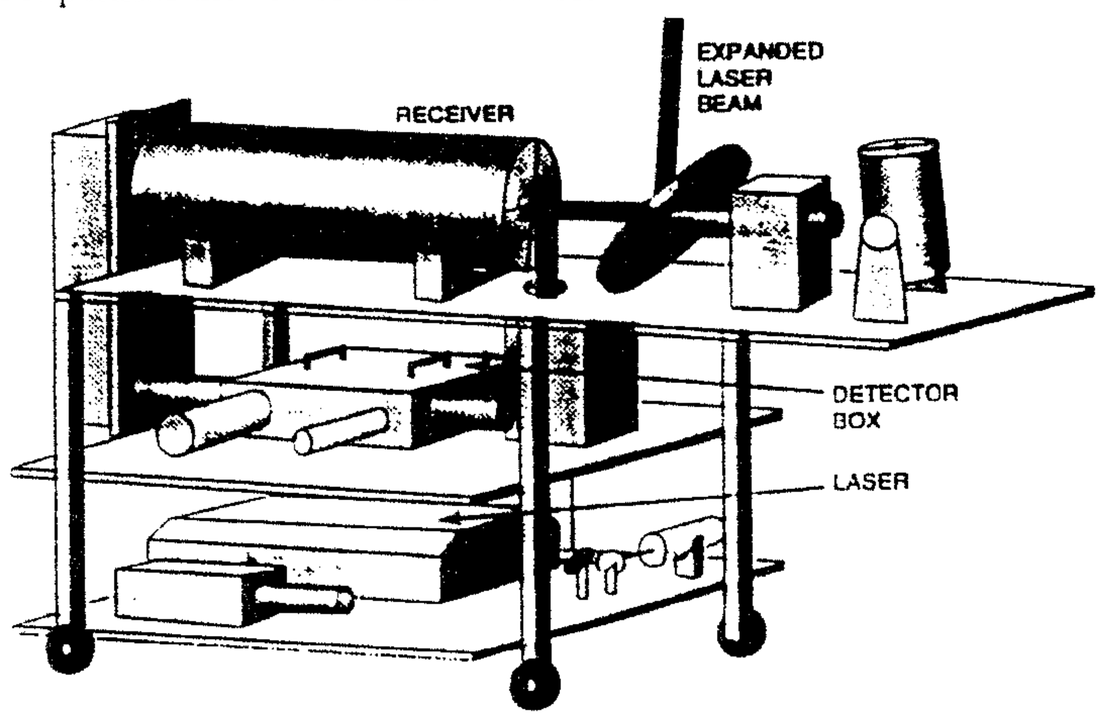

Figure 3. A diagram of the LAMP lidar shows the laser on the bottom of the table, the detector on the middle shelf, and the receiving telescope at the top with the beam steering mirror.

The Nd:YAG laser has an output of 1.5 j at 20 Hz at the 1064 nm fundamental output. The beam is passed through a doubling crystal and a mixing crystal to produce the 532 and 355 nm, or 266 nm, beams which are used for the lidar measurements. The primary receiver is a 42 cm diameter Cassegrain telescope. The low altitude backscatter signals of the visible and ultraviolet beams can be detected as analog signals and digitized at 10 MSps to provide 15 meter resolution from the surface to 25 km, or detected as photon count signals with 75 m altitude resolution. The high altitude signals, obtained by photon counting techniques, are accumulated into 500 nanosecond range bins to provide 75 meter resolution, from 20 to 80 km. The high altitude detector also contains low altitude photon counting channels which measure the first Stokes vibrational Raman signals of the N_2 and the H_2O Raman scatter. The low altitude detector has eight channels to measure the backscatter signal at two laser fundamental lines, two N_2 Raman lines, two H_2O water vapor lines and two segments of the rotational Raman envelope. The transmitter, receiver, detector, and data system combination have been integrated into a standard shipping container, which serves as a field laboratory. We have investigated the possibility of measuring the temperature profile in the turbid lower atmosphere using the N_2

vibrational Raman signal. However, this approach has proven to be quite limited due to the accuracy with which the extinction can be determined when cloud layers are present [Rau (1994)]. However, measurements of the rotational Raman backscatter have proven to be the appropriate way to measure the temperature profiles in the presence of clouds, aerosols, and in the boundary layer.

Refractivity Measurements

Lidar measurements of coastal atmospheric refractive environments were made during the 1993 Summer and Fall VOCAR (Variability of Coastal Atmospheric Refractivity) Campaigns, with the lidar situated at Pt. Mugu, CA. The lidar derived refractivity profiles are analyzed for refractive layer structures and the EM wave propagation environment in the Southern California near-coastal region. During the summer at Pt. Mugu, humid atmospheric conditions near the surface, accompanied by temperature inversion layers, produced periods of intense refractive ducting (EM wave trapping) affecting VHF and UHF radio signals which were also monitored during VOCAR. The signal levels received, from several (existing) airport ATIS & MCAS transmissions, and (installed) CW radio transmitters at the San Clemente Is. These propagation paths provided a means of investigating the propagating conditions. The receiving and recording systems were located at Pt. Mugu and San Diego. A wide range of received signal levels (exceeding 40 dB propagation loss variations) were experienced over weeks of operational data collection. The ocean and coastal radio paths are analyzed for path signal levels and signal amplitude variability. The propagation conditions were modeled through the use of the RPO, IREPS, EREPS propagation programs.

The coincident lidar derived refractivity measurements have been analyzed for temporal variability and to provide the input of propagation environmental conditions for the models. Rapid succession lidar derived profiles permitted the examination of the short term (hour-to-hour) variations throughout a day (30 minute integrations used). The refractive layer temporal structure and vertical stratifications are examined in detail.

OBSERVATIONS

Basic Measurements of Refractive Index

A series of lidar refractivity profiles on five night-to-day periods during the 26-31 August 1993 have been analyzed to examine temporal and vertical structure and variation. Examples of the basic measurement profiles of water vapor (specific humidity, g/kg) and temperature (deg. K) are shown in Figures 4 and 5 respectively, with near-time radiosonde profiles on 26 August. The resulting refractivity (N), Figure 6, and modified refractivity (M), Figure 7 profiles are shown for altitudes of 0-1500 m for three 30 min. time accumulation periods. The rapid drop in water vapor with altitude coincides with the temperature inversion (positive lapse rate) profile, Figure 5, to produce a strong trapping layer to heights of 600 m on August 26th., (350 m on August 27th.).

Time History (26-31 Aug. '93 - Pt. Mugu PSU Lidar)

A sample of the data series is given in Figures 8 and 9, in terms of 3-D surface plots of refractivity, N and modified refractivity M on 26 August. During this period, strong ducting was occurring and UHF radio signals were enhanced on a long beyond-the-horizon 132 km path over the ocean (San Clemente Is.-to-Pt. Mugu) to levels exceeding the free space (line-of-sight) condition. The temporal and altitude structure are evident, showing stable (persistent) conditions of surface-based ducting over long periods of more than two days. Analysis of the 26-27 Aug. data has been performed (Helvey,1994), indicating that the M-profile refractive duct height and temporal history agrees with that derived from longer term radiosonde sampling throughout the same period. The detailed structure reveals sub layers which appear and fade somewhat throughout the time period. Figure 10 indicates the prevailing ducting conditions on 27 August (strong negative N gradient from the surface).

As the days progressed, the refractive conditions gradually changed to elevated ducts and eventually to no significant ducting on 31 August (Figures 11, 12, and 13, for 28, 29, & 31 August, respectively). Sample N and M profiles from these five days are given in Figures 14 to 18, where the existence of ducting or non-ducts can be easily identified on each day. Figures 14 and 15 show that conditions of surface-based ducting occurred (26, 27 Aug.). Figure 16 shows that the conditions have changed to an elevated, but surface based duct (28 Aug.). On August 29th, Figure 17 shows that an elevated duct only exists, and therefore surface level only propagation will not encounter trapping. An elevated antenna system within the duct at about 425 meters, will incite guided wave propagation and possible coverage holes above and below the layer. Finally, by 31 August, Figure 18, there is little evidence of ducting

occurring at any height.

Application of N-Profiles to Propagation Models

Given the measured refractivity profile(s), analysis of propagation path losses, raytracings and guided-mode wave propagation can be accomplished through the use of the Navy's IREPS (Hitney,1985), EREPS (Hitney, 1989), and RPO (Radio Physical Optics, Paulus, 1994) propagation models & analysis PC programs. An example of the use of the use of RPO with a single vertical refractivity profile from the Pt. Mugu Lidar is given in Figure 19. The figure coverage/loss plot for emissions from an arbitrary S-band system shows the existence of a near-surface propagation waveguide condition during surface based ducting, with signal leakage at modal (reflection) points along the path.

Radio Measurements and Model Predictions

The long term (day-to-day) effects show correlation between over all high signal levels and the presence of persistent surface-based ducts as measured with the Lidar. The strongest signal levels on beyond-the-horizon paths can reach or exceed free space propagation predictions from San Clemente Is.-to-Point Mugu (at UHF, 375 MHz, Figure 20). The VHF (143 MHz) received signal, though enhanced over non-ducting conditions, did not exceed the line-of-sight (free space) level (see Figure 21). It should be noted that the UHF and VHF amplitude variations, however, are highly correlated. The peak-to-minimum signal level variability can range over 40 dB during an eight day period preceding and including the 26 & 27 August operations, as indicated in the figures. Raypath propagation can be examined with IREPS coverage displays (Figures 22 and 23 for the UHF and VHF extended range propagation on 26 August), and by EREPS raypath propagation (Figure 24). Quantitative propagation losses, however are difficult to obtain with a high degree of accuracy using these programs alone.

The more detailed propagation loss structure can be analyzed through the use of RPO (NRaD's Radio Physical Optics program). Examples of RPO output in terms of color contour (or shaded) dB losses are given in Figures 25 and 26 for a 26 August (1013 UT) lidar profile and the SCI-to-Pt. Mugu UHF (374.9 MHz) and VHF (143.1 MHz) signal frequencies. Then the propagation loss profile can be displayed as a function of range (constant height) or height (constant range). Figure 27 shows the height variation at 132 km range for the preceding path and time. Figure 28 shows the range variation for a receiving antenna at 30.5 meters (the height used at Pt. Mugu). The propagation excess losses at 132 km for the two frequencies are at +2.5 dB for UHF, and -14 dB for VHF, below free space losses, ie., at the approximate received signal levels indicated in Figures 20 and 21 respectively on August 26th (Julian date 238). Analysis of the other days of the five day period also show good agreement between predictions and observations for surface, elevated ducting, and non-ducting conditions.

SUMMARY

The lidar instrument provides input for rapid refractive index profiling and detailed propagation analysis of refractive effects on EM systems. The testing at Point Mugu has verified the performance of lidar as a point location profiler of the tropospheric refractivity state. The lidar data output has been formatted to radiosonde standards and therefore provides input to existing propagation analysis software. Refractivity conditions processed and analyzed to date have provided data that has spanned a wide variety of propagation conditions ranging from strong ducting to non-ducting in the near-surface refractive environments of Point Mugu, CA. These measurements have been applied to predictions for the long ocean path from San Clemente Is.-to-Point Mugu. Good correspondence has been found between lidar derived refractivity profiles input to the RPO model for signal level prediction, and signal level observations at UHF and VHF during the VOCAR campaign test periods.

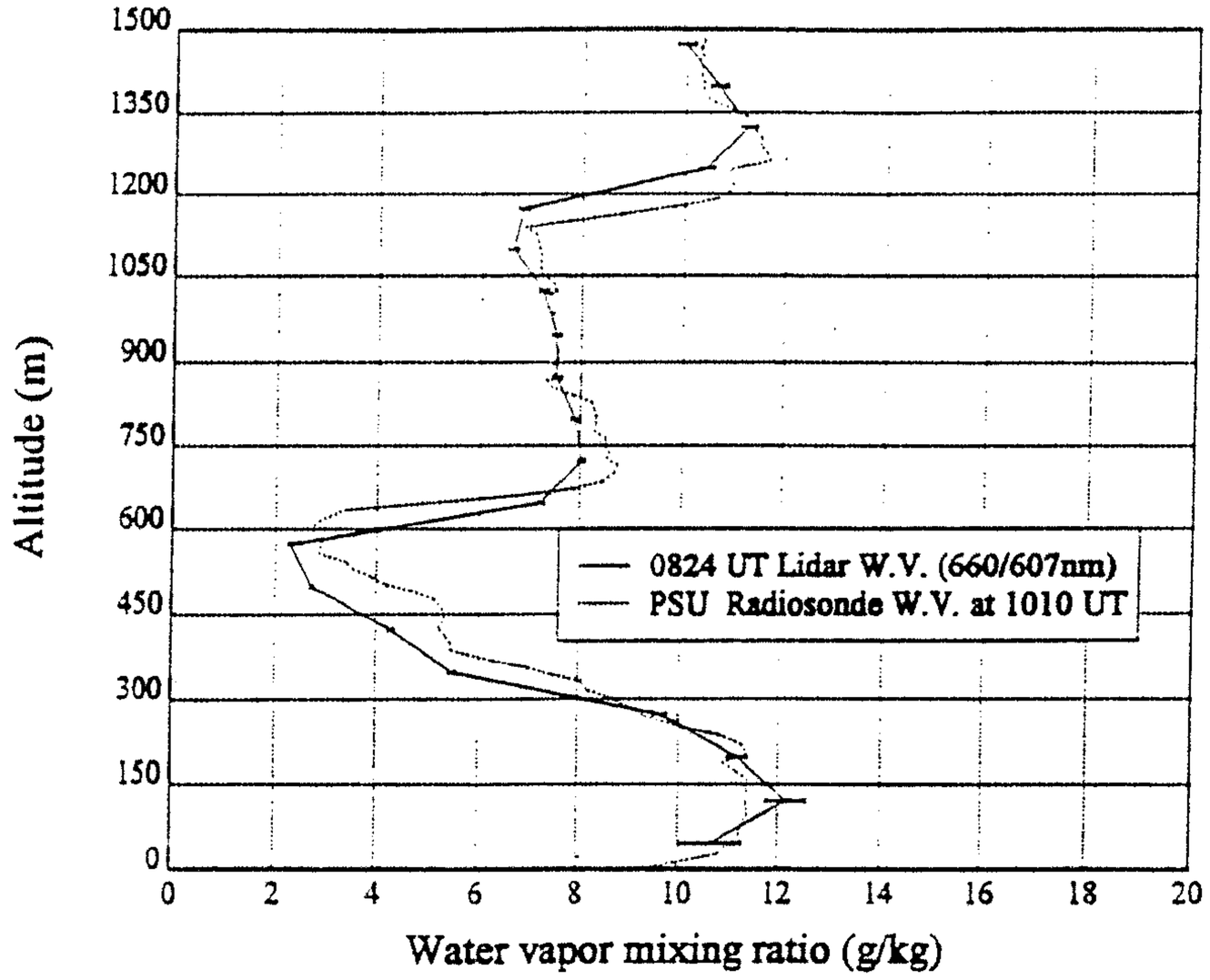

Figure 4. Water vapor profiles measured by lidar and rawinsonde balloon at 0824 UT on 26 August 1993.

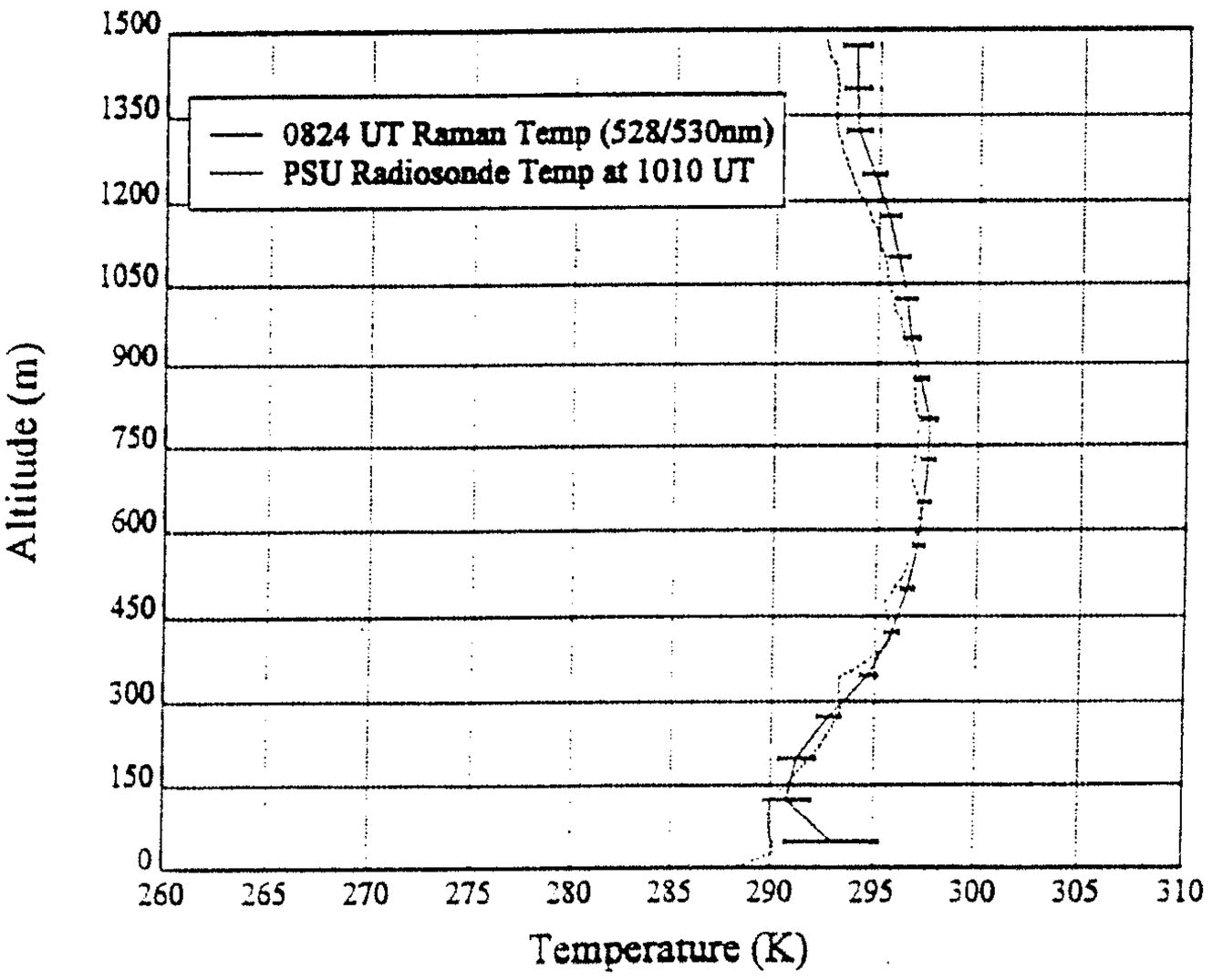

Figure 5. Temperature profiles measured by lidar and rawinsonde balloon at 0824 UT on 26 August 1993.

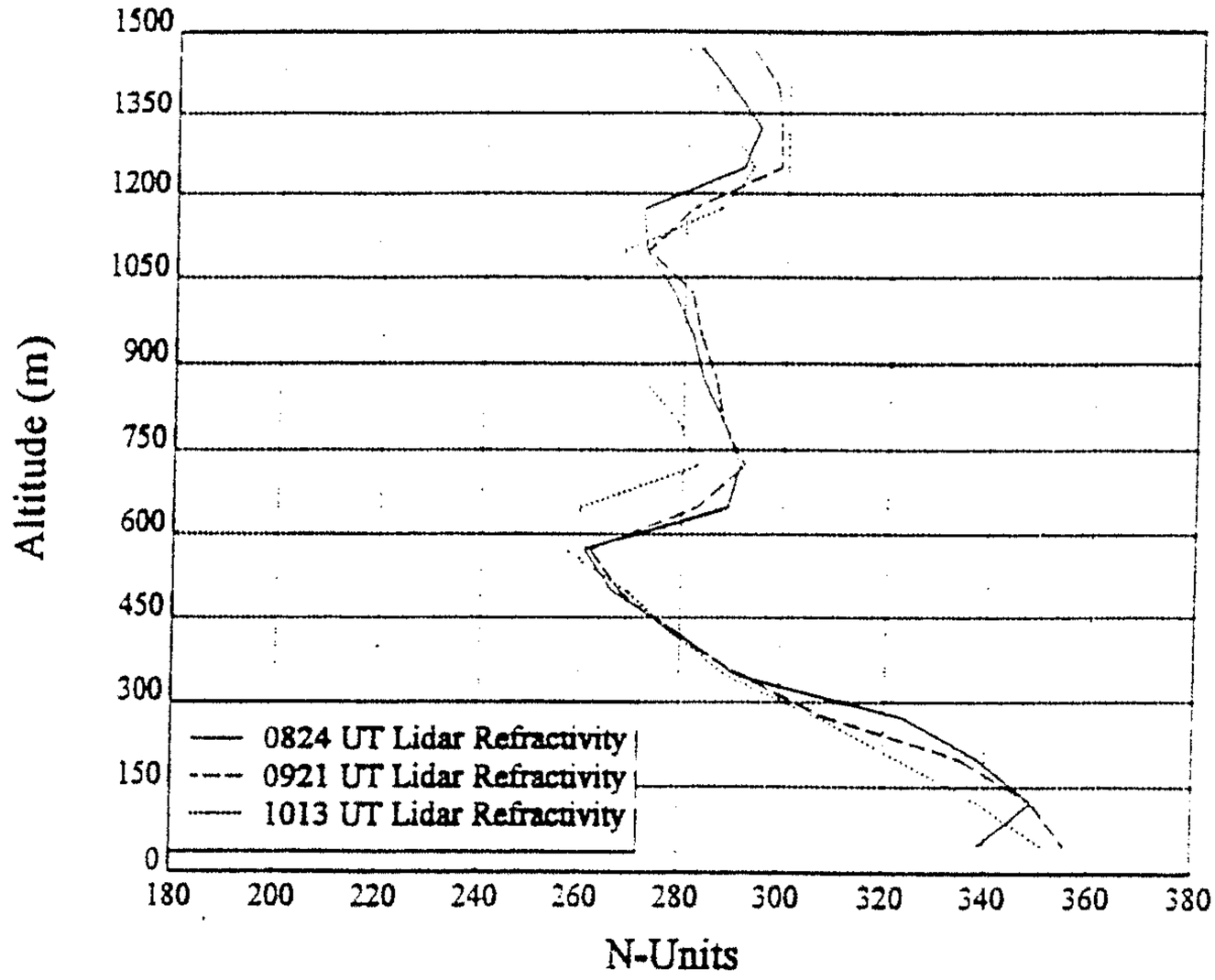

Figure 6. Refractivity profiles derived from lidar data at 0824, 0921 and 1013 UT on 26 August 1993.

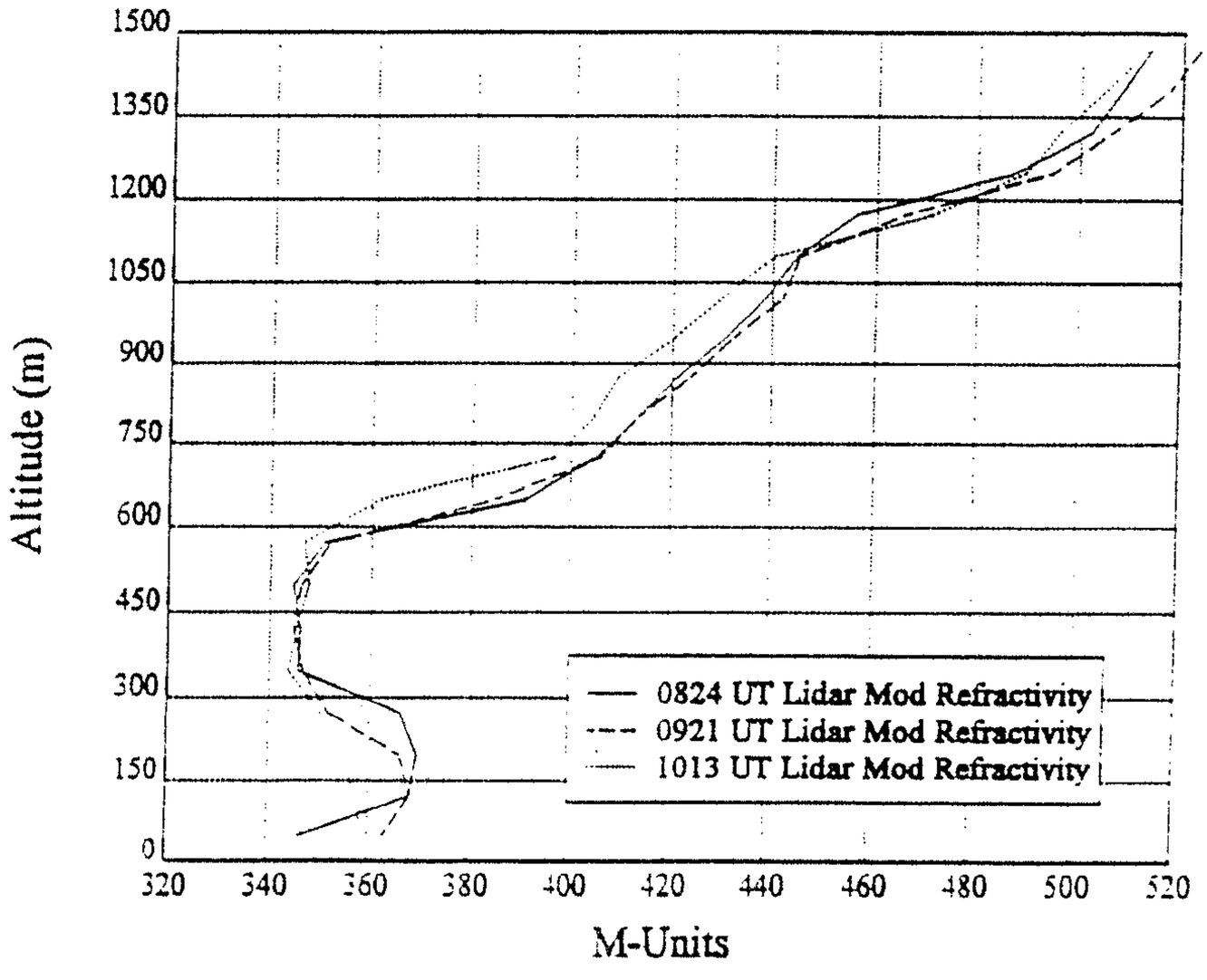

Figure 7. Modified refractivity profiles derived from lidar data at 0824, 0921 and 1013 UT on 26 August 1993.

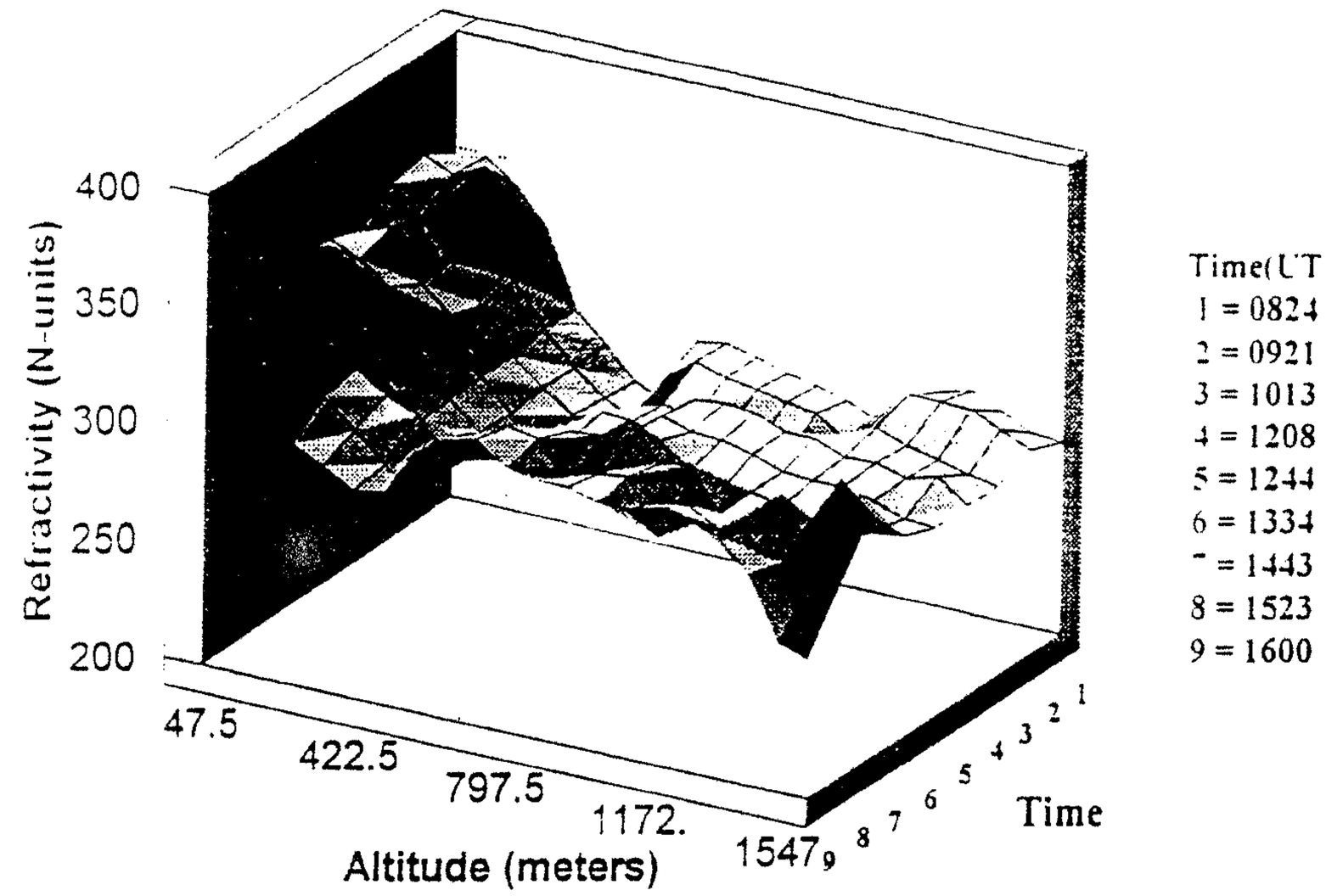

Figure 8. Refractivity surface contour as a function of time on 26 August 1993.

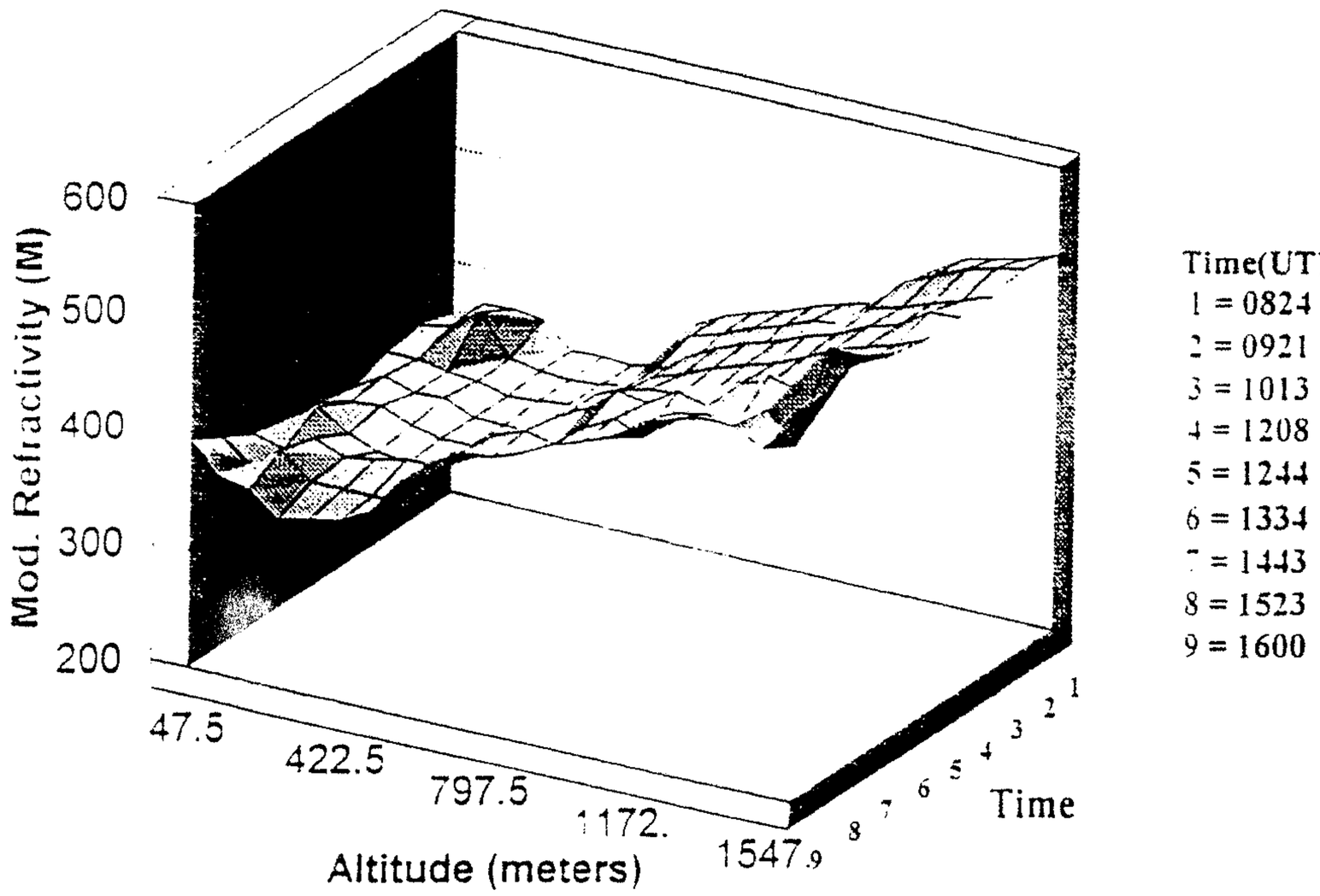

Figure 9. Modified refractivity surface contour as a function of time on 26 August 1993.

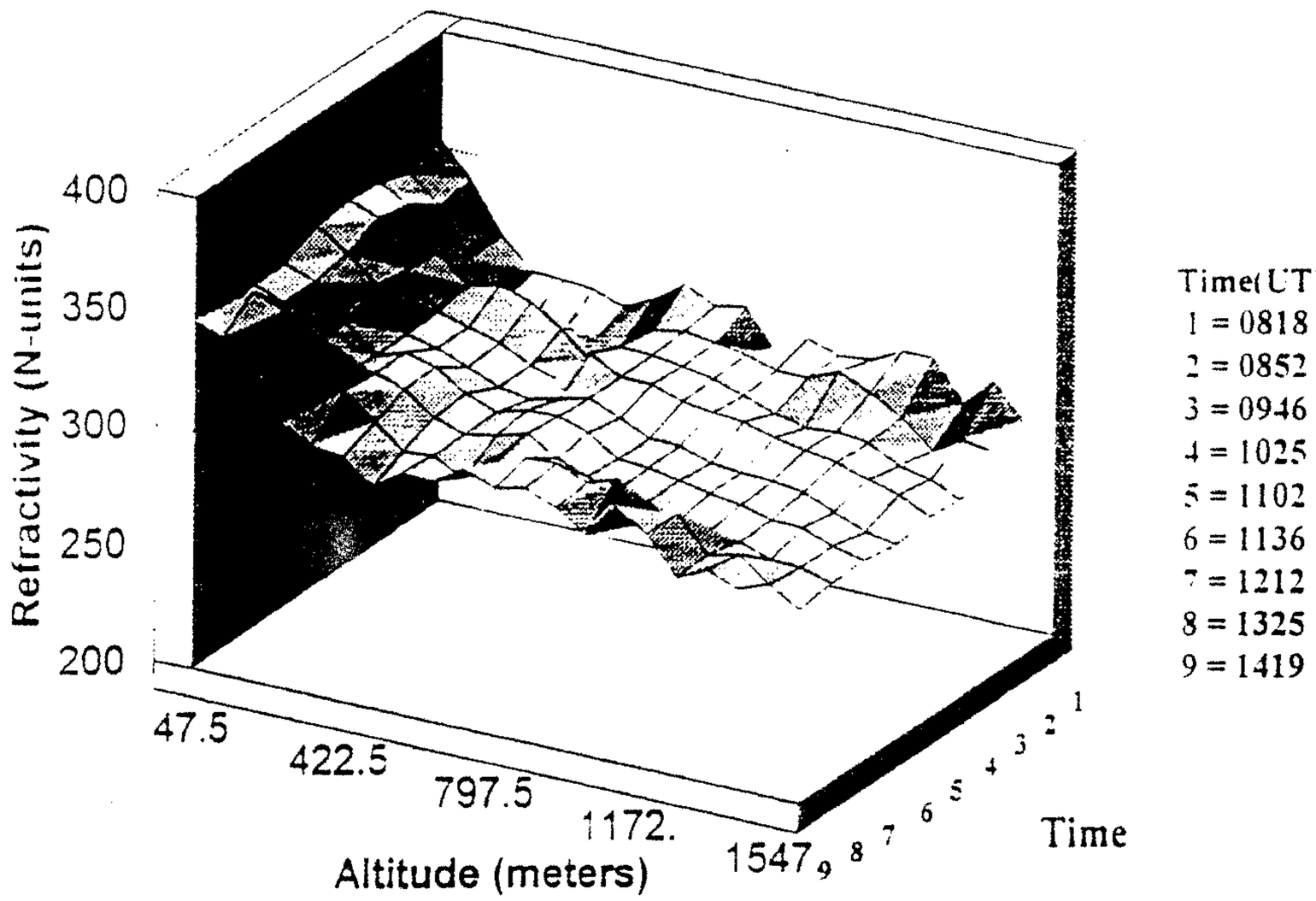

Figure 10. Refractivity surface contour as a function of time on 27 August 1993.

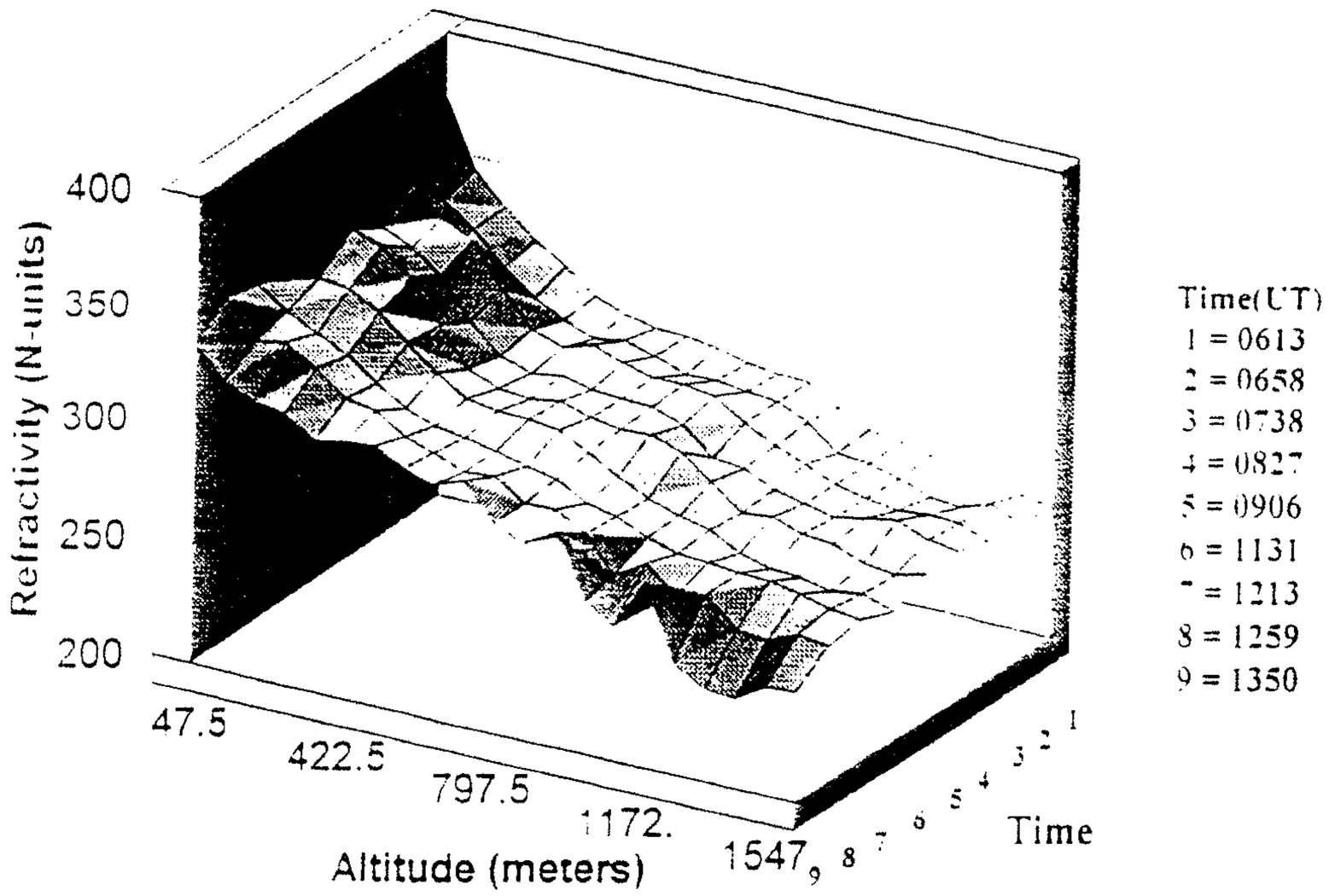

Figure 11. Refractivity surface contour as a function of time on 28 August 1993.

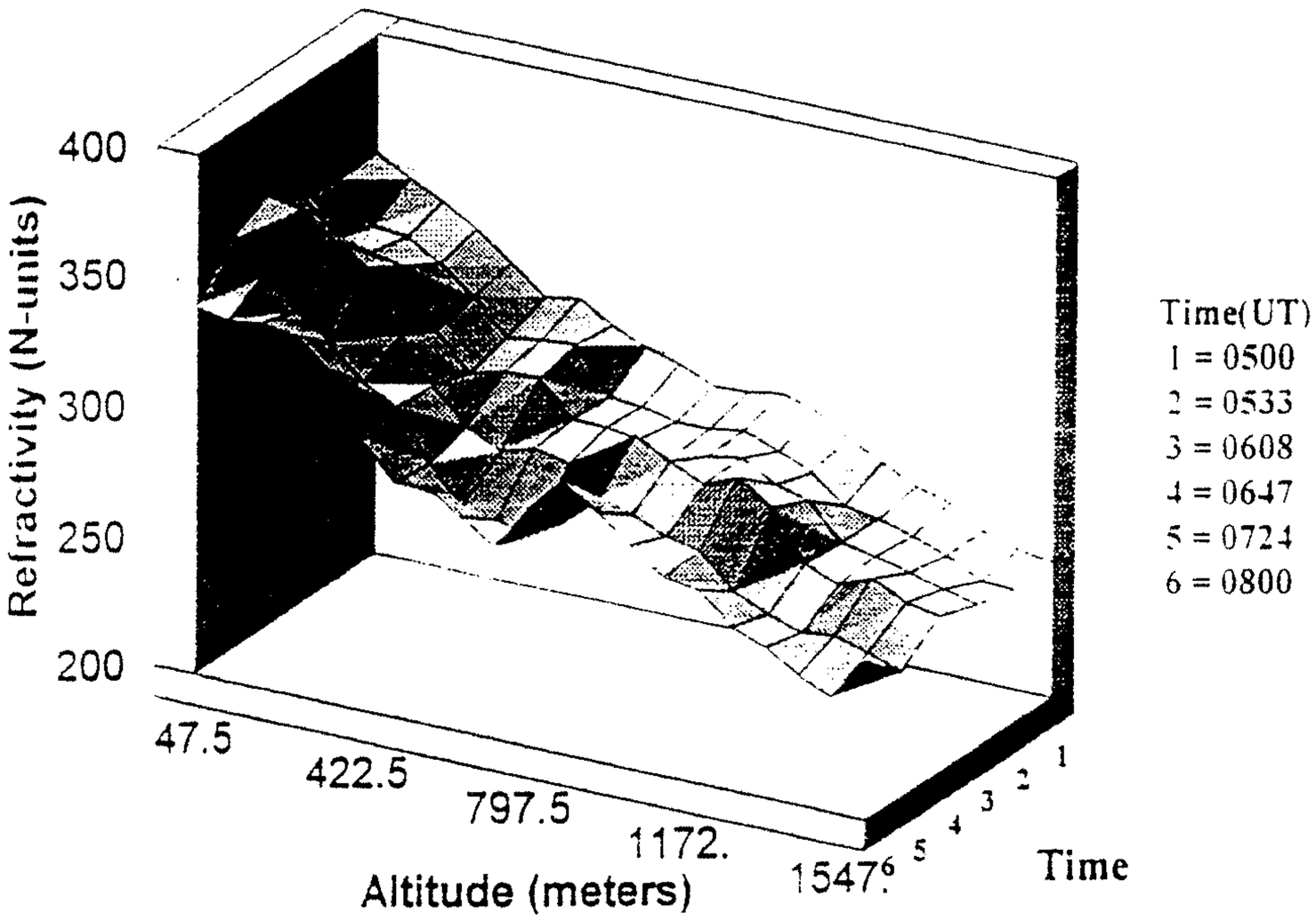

Figure 12. Refractivity surface contour as a function of time on 29 August 1993.

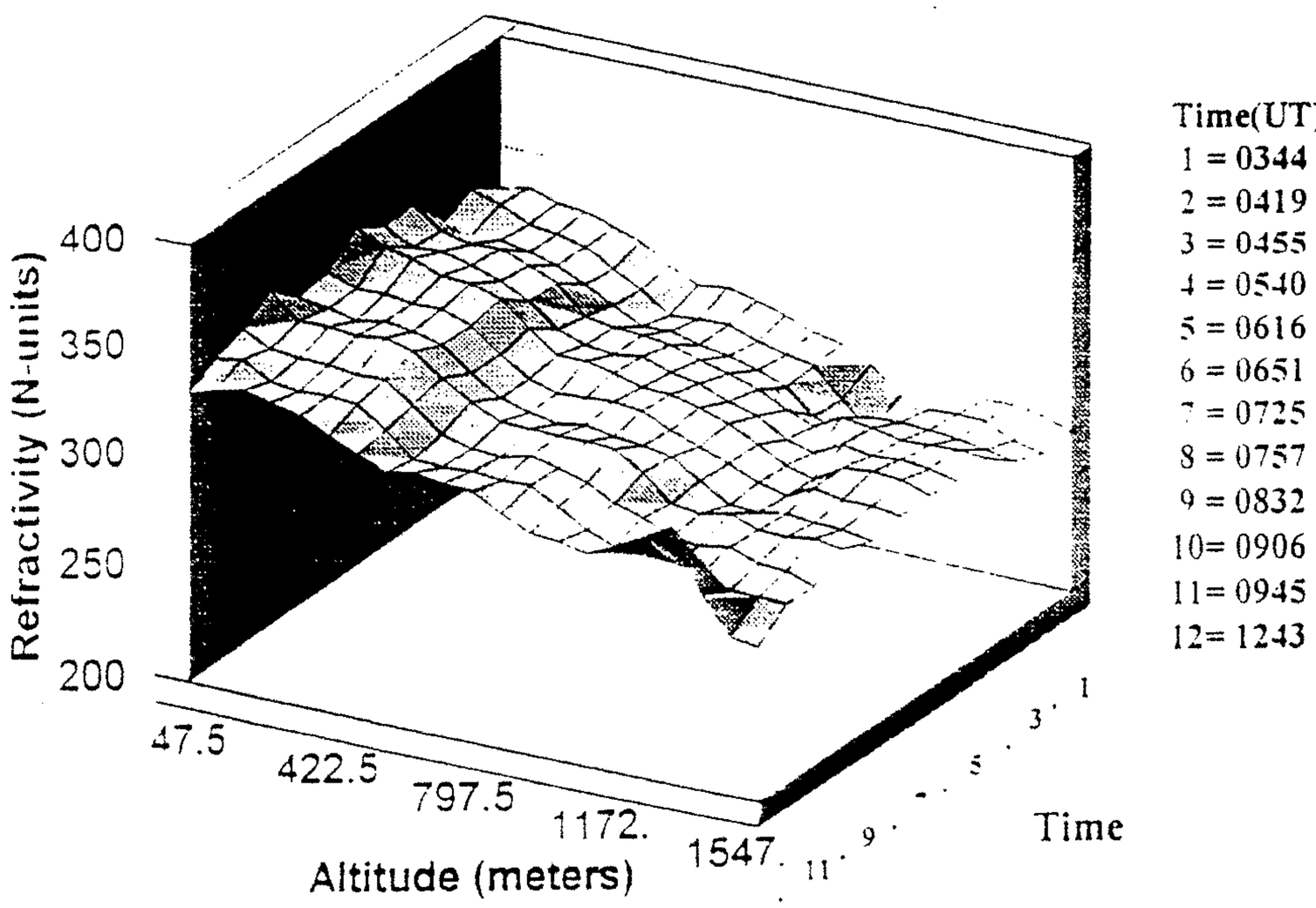

Figure 13. Refractivity surface contour as a function of time on 31 August 1993.

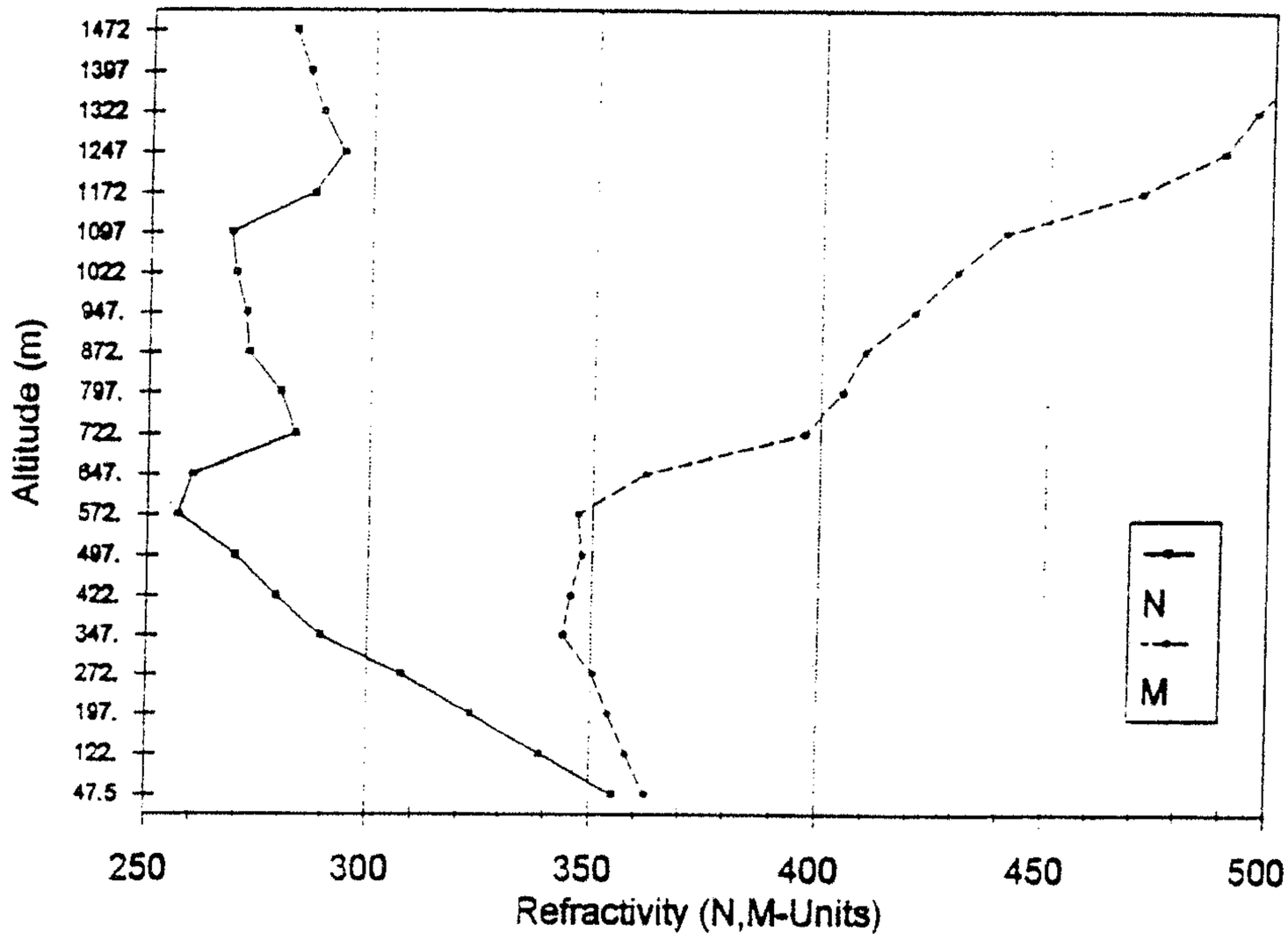

Figure 14. Refractivity and modified refractivity profiles from lidar results show a surface-based duct to 600 m height at 1013 UT on 26 August 1993.

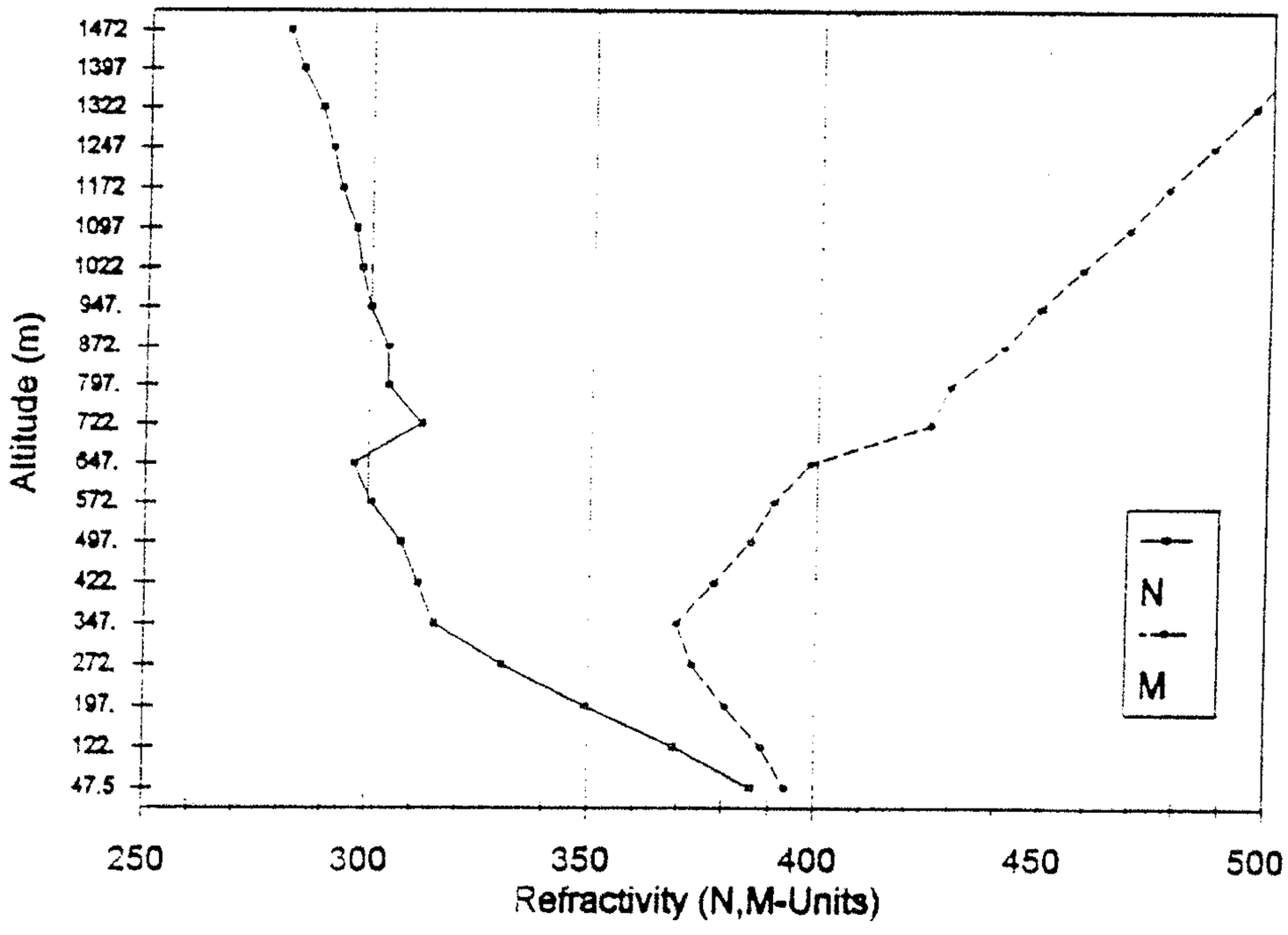

Figure 15. Refractivity and modified refractivity profiles from lidar results show a surface-based duct to 350 m height at 1025 UT on 27 August 1993

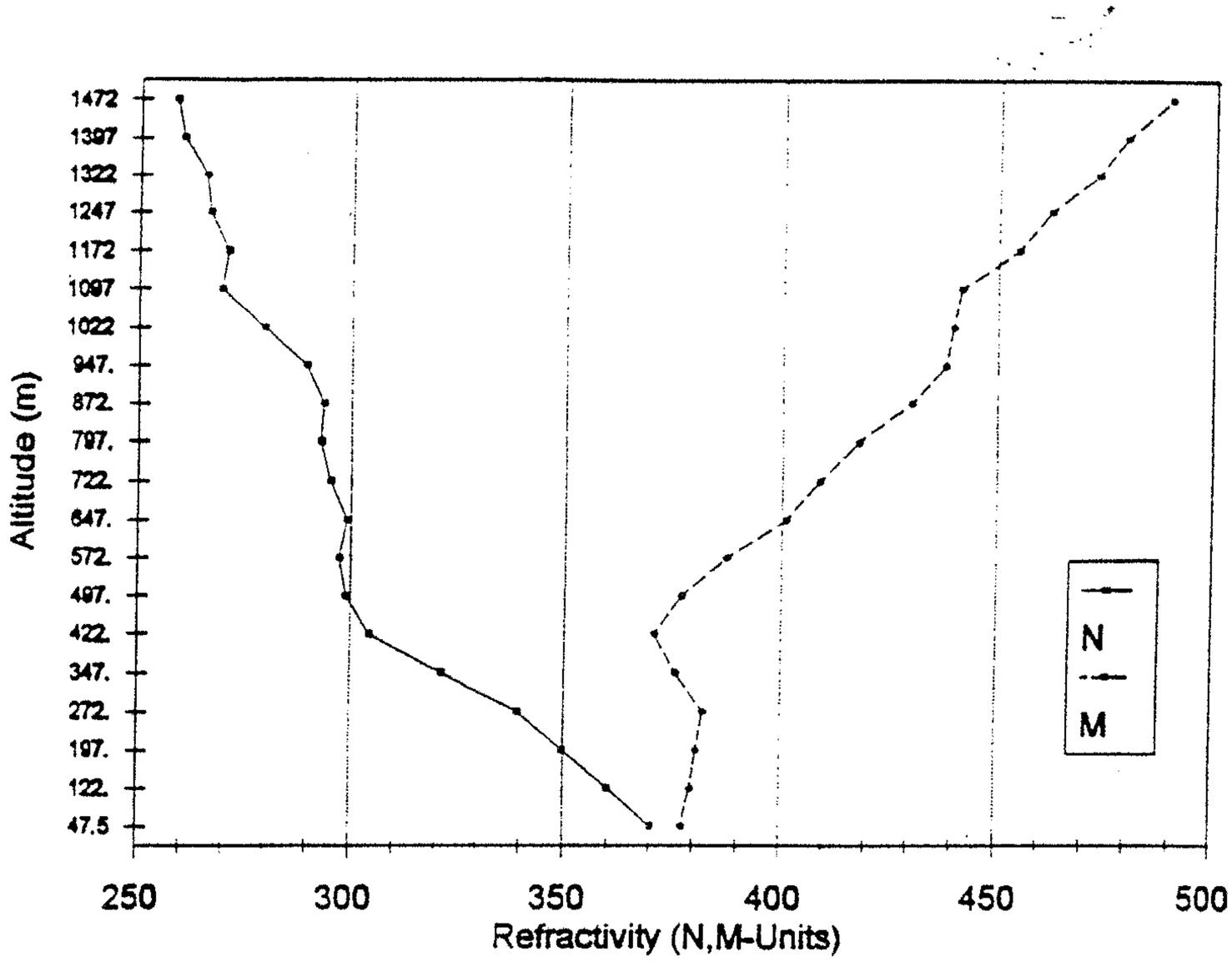

Figure 16. Refractivity and modified refractivity profiles from lidar results show a surface-based duct to 425 m height at 0906 UT on 28 August 1993.

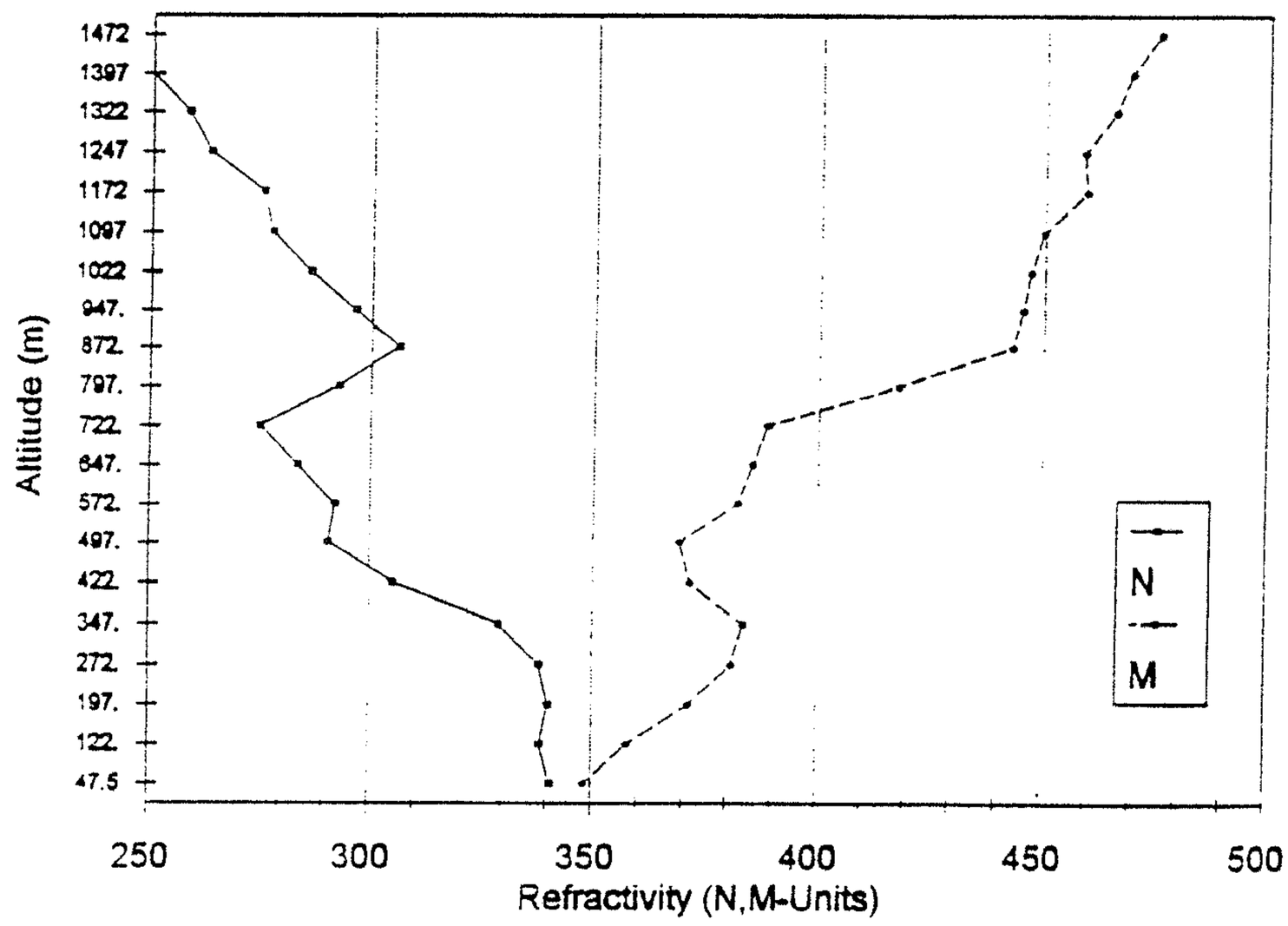

Figure 17. Refractivity and modified refractivity profiles from lidar results show an elevated duct at 350 to 500 m heights at 0800 UT on 29 August 1993.

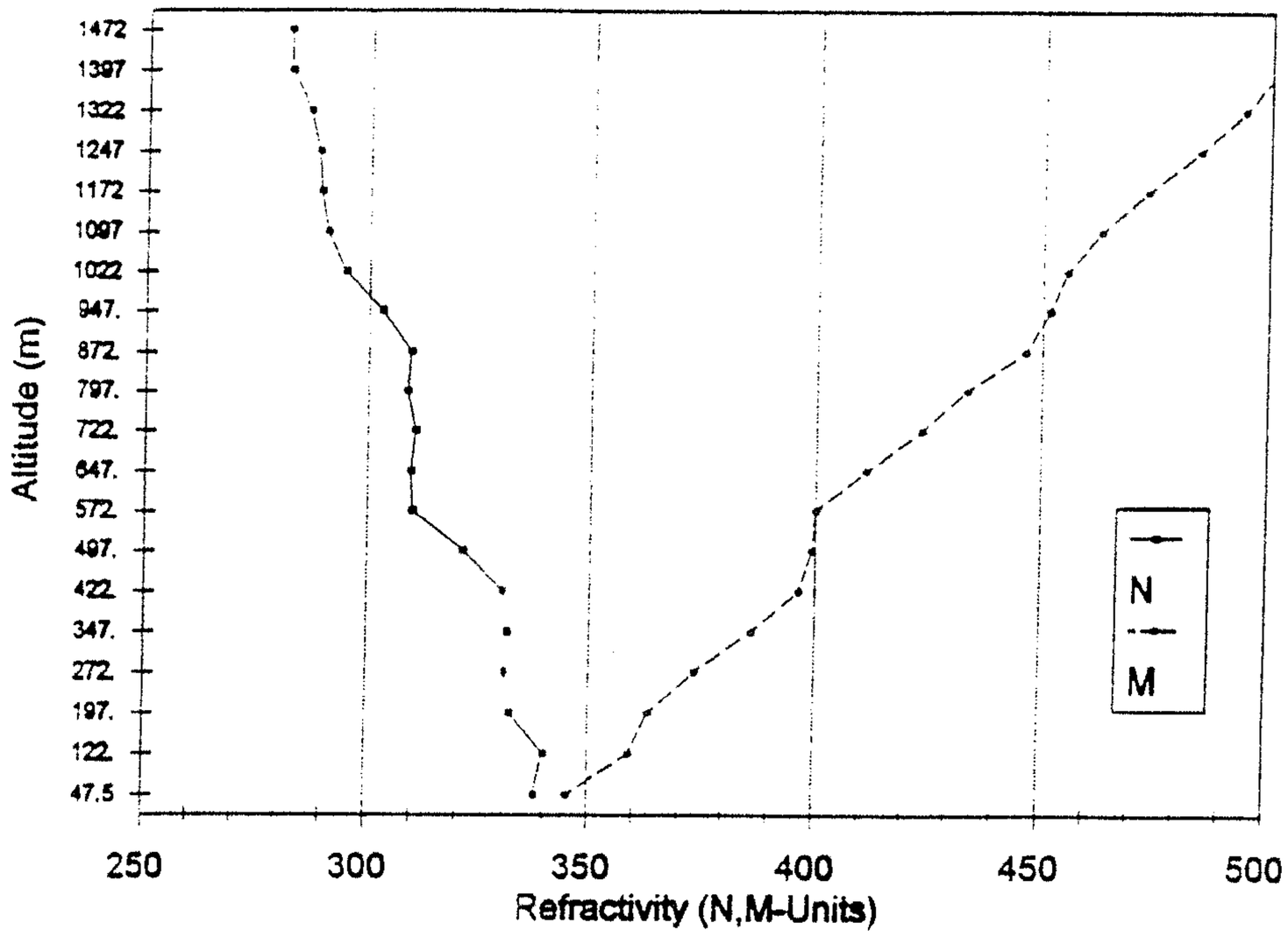

Figure 18. Refractivity and modified refractivity profiles from lidar results show non-ducting conditions (non-anomalous) at 0945 UT on 31 August 1993.

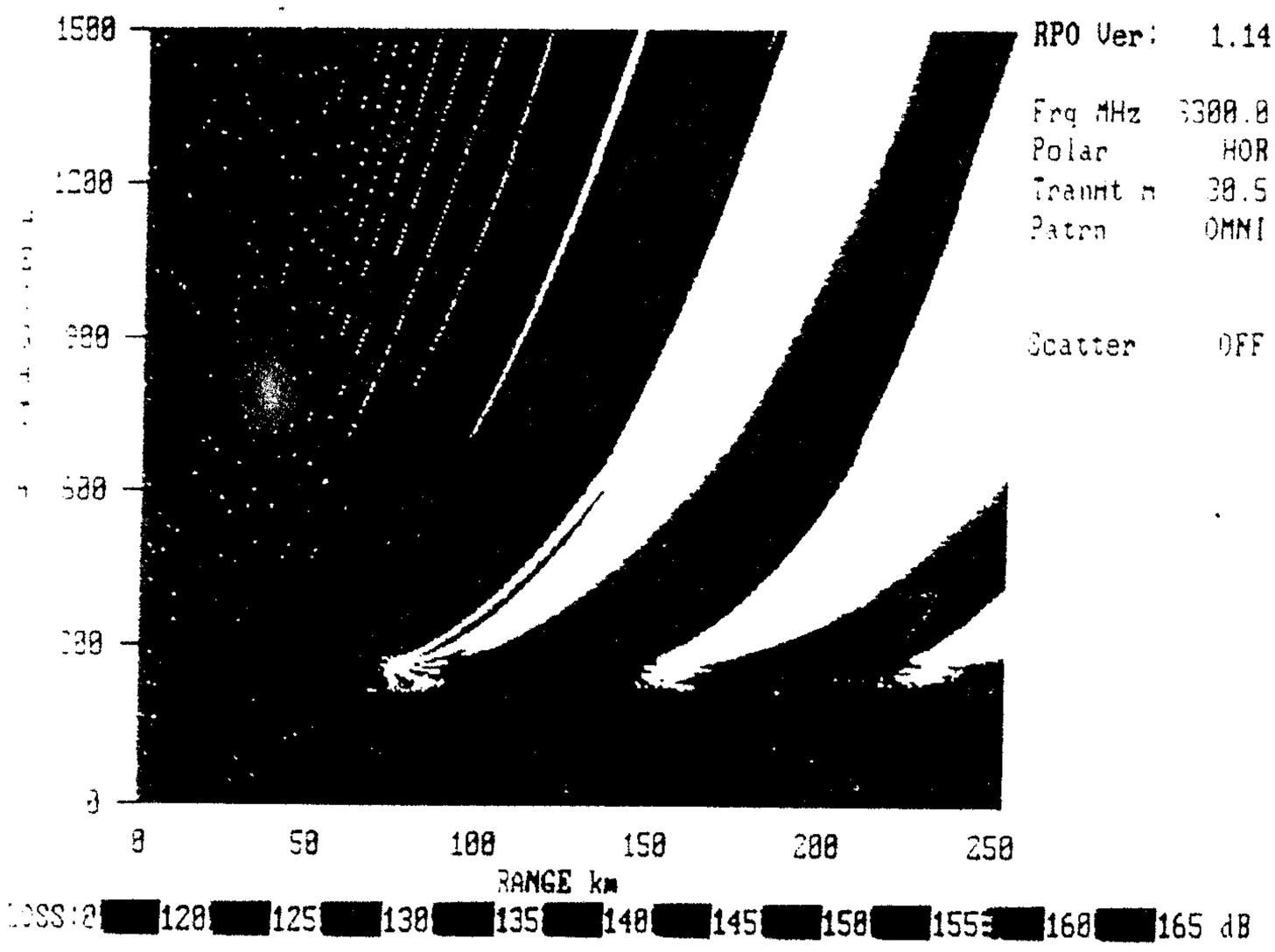

Figure 19. Propagation coverage diagram from RPO model based on lidar results at 1013 UT on 26 August 1993.

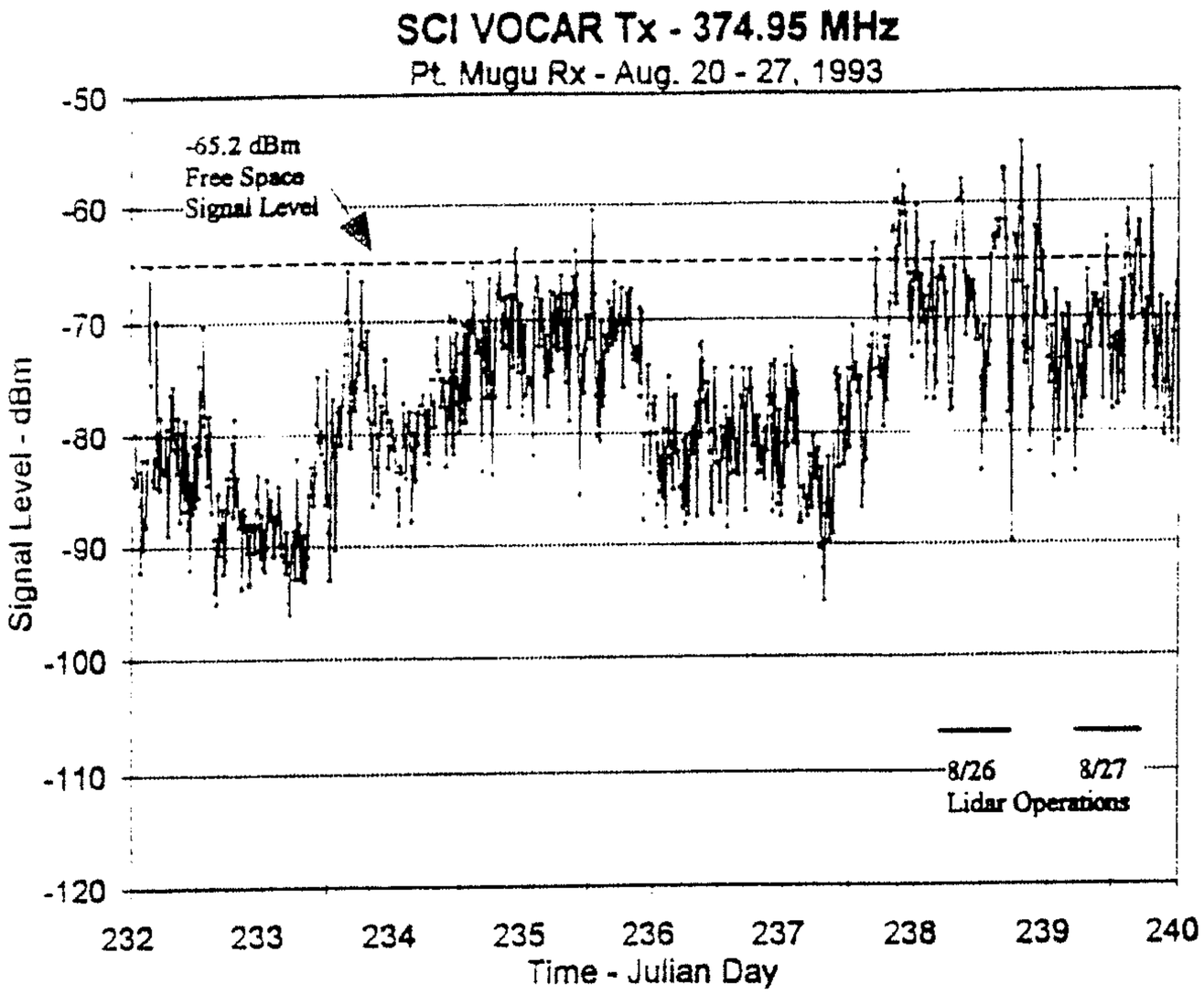

Figure 20. Measured VOCAR received UHF signal level over 132 km ocean path from San Clemente Island to Point Mugu during an 8 day period in late August 1993.

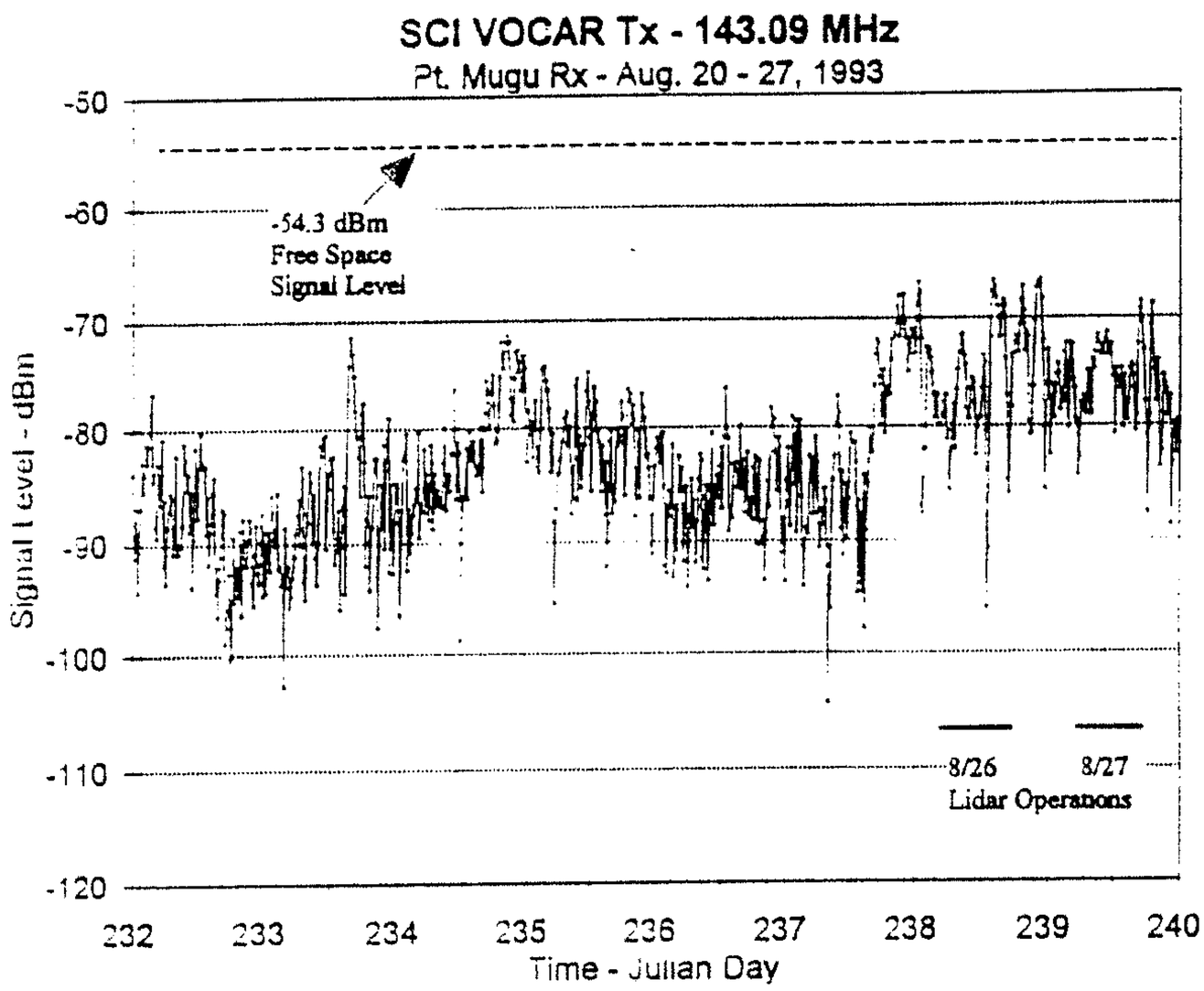

Figure 21. Measured VOCAR received VHF signal level over 132 km ocean path from San Clemente Island to Point Mugu during an 8 day period in late August 1993.

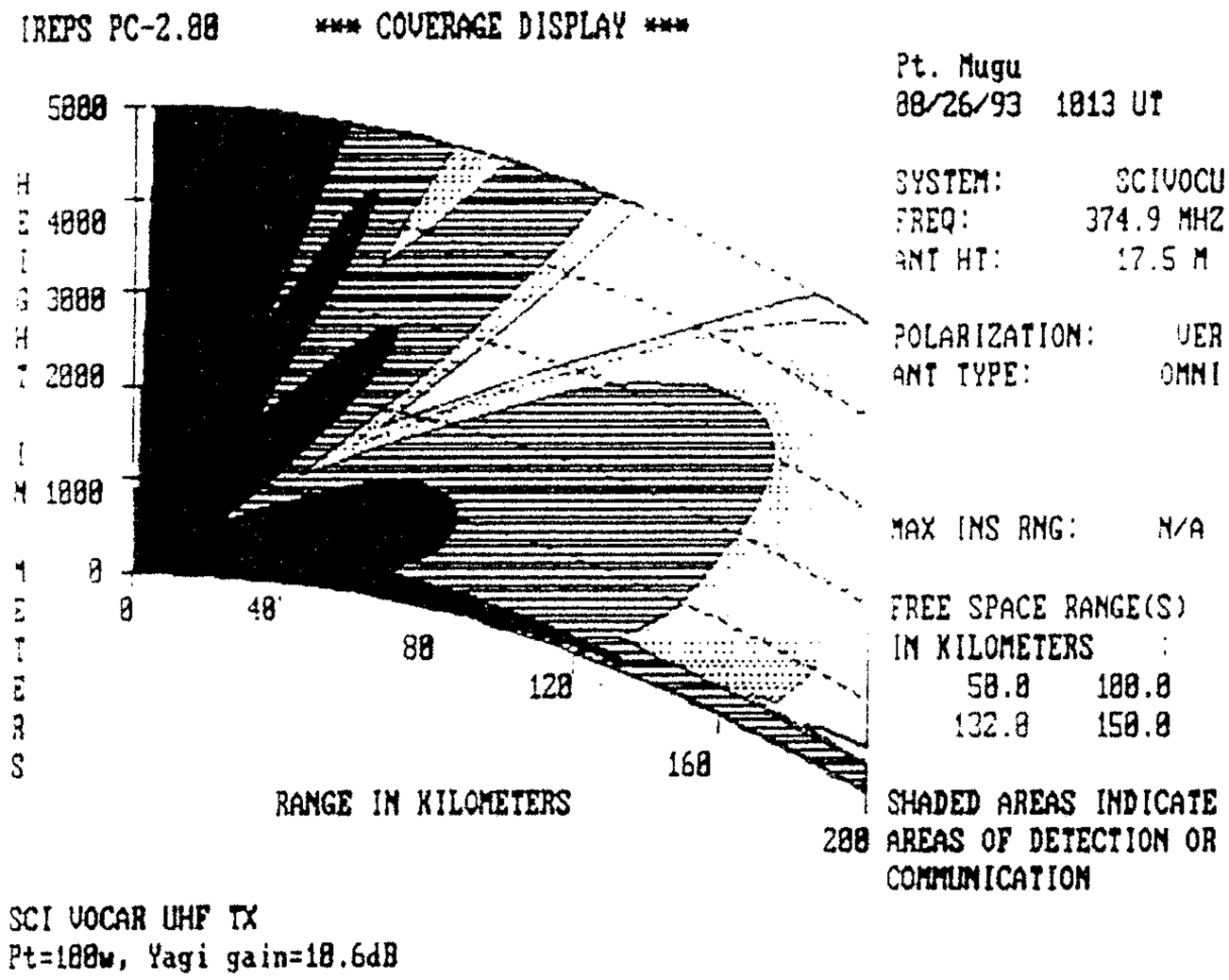

Figure 22. Output from IREPS at UHF using lidar profiles for 1013 UT on 26 August 1993.

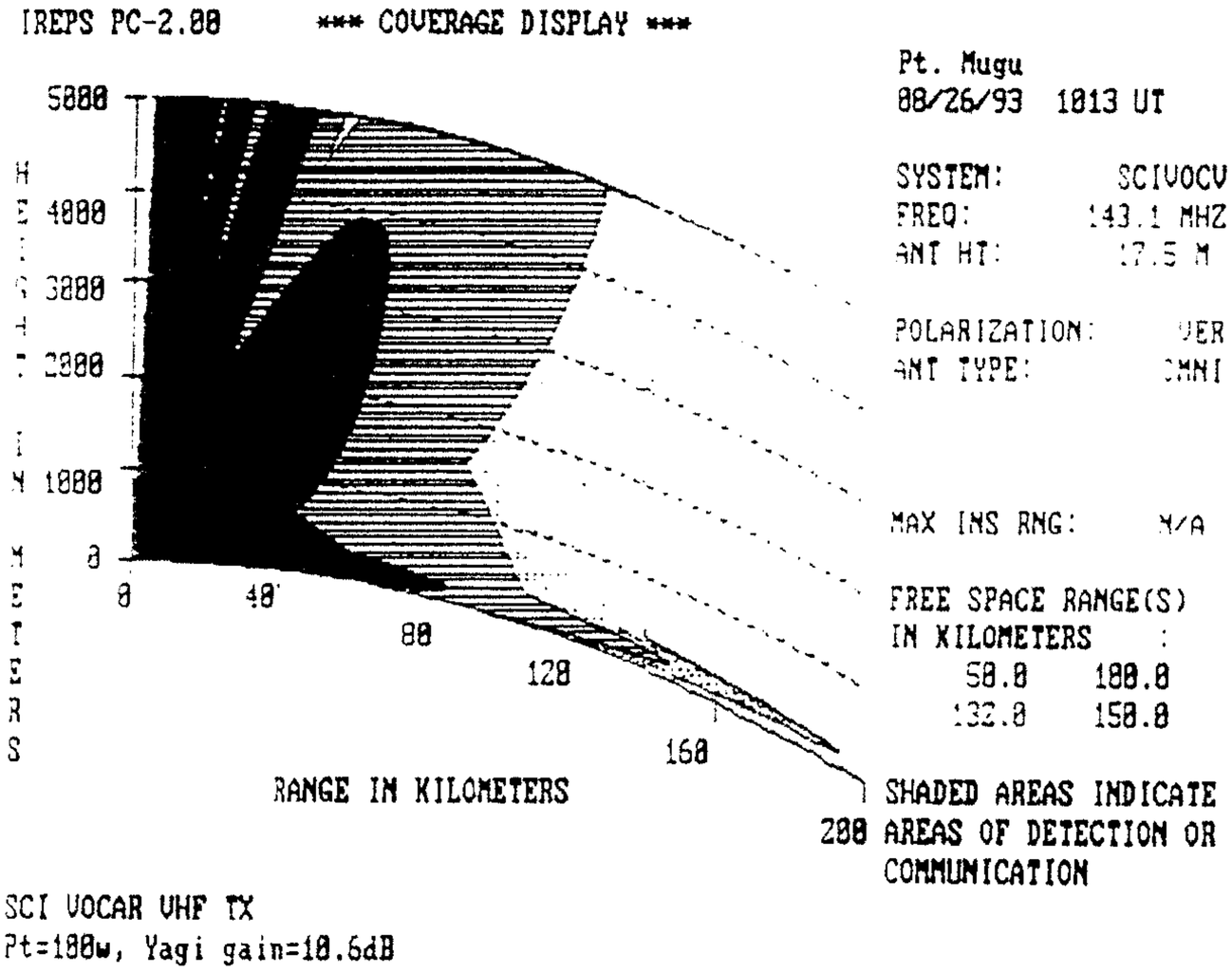

Figure 23. Output from IREPS at VHF using lidar profiles for 1013 UT on 26 August 1993.

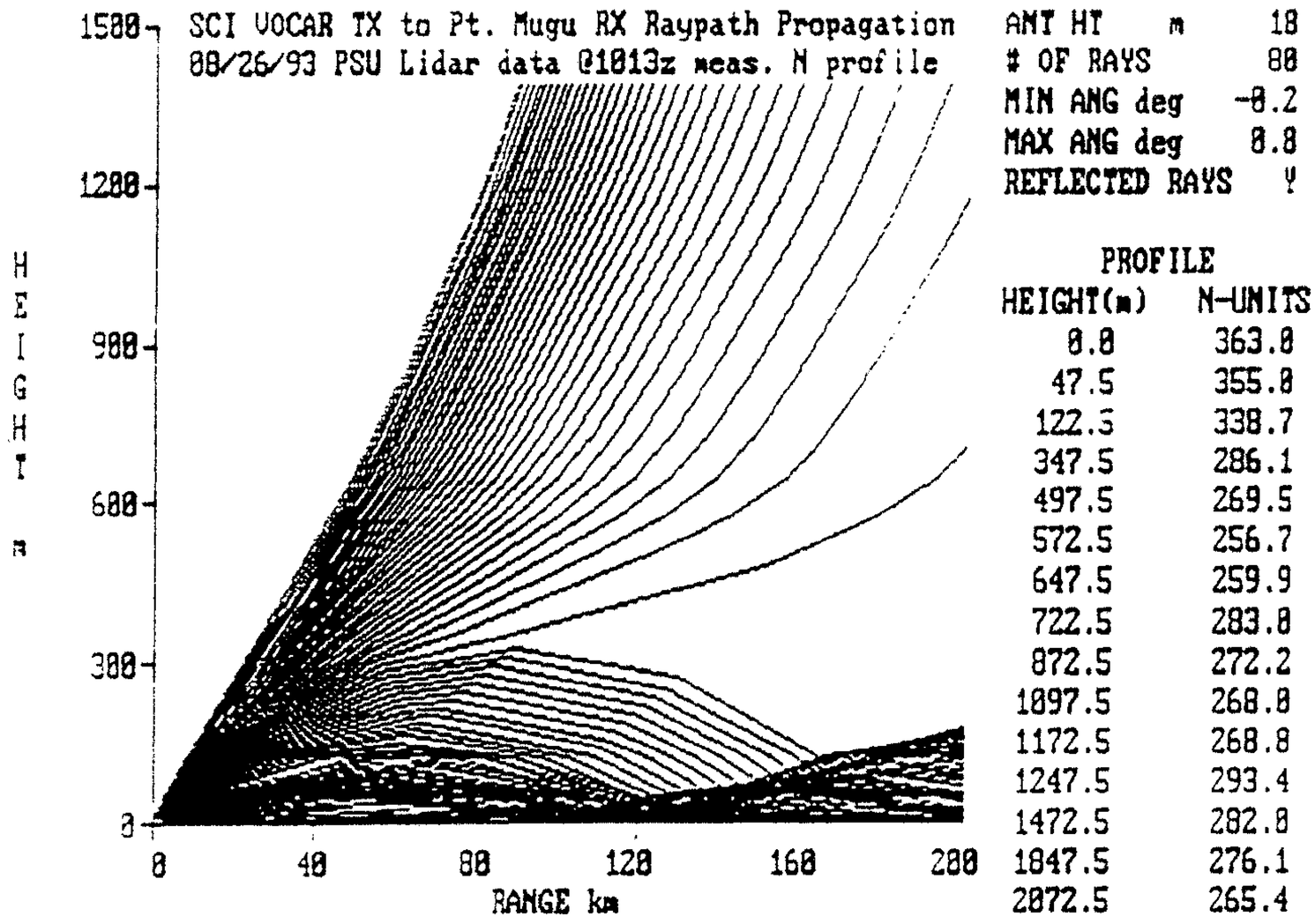

Figure 24. Raytracing output from EREPS using the lidar results at 1013 UT on 26 August 1993.

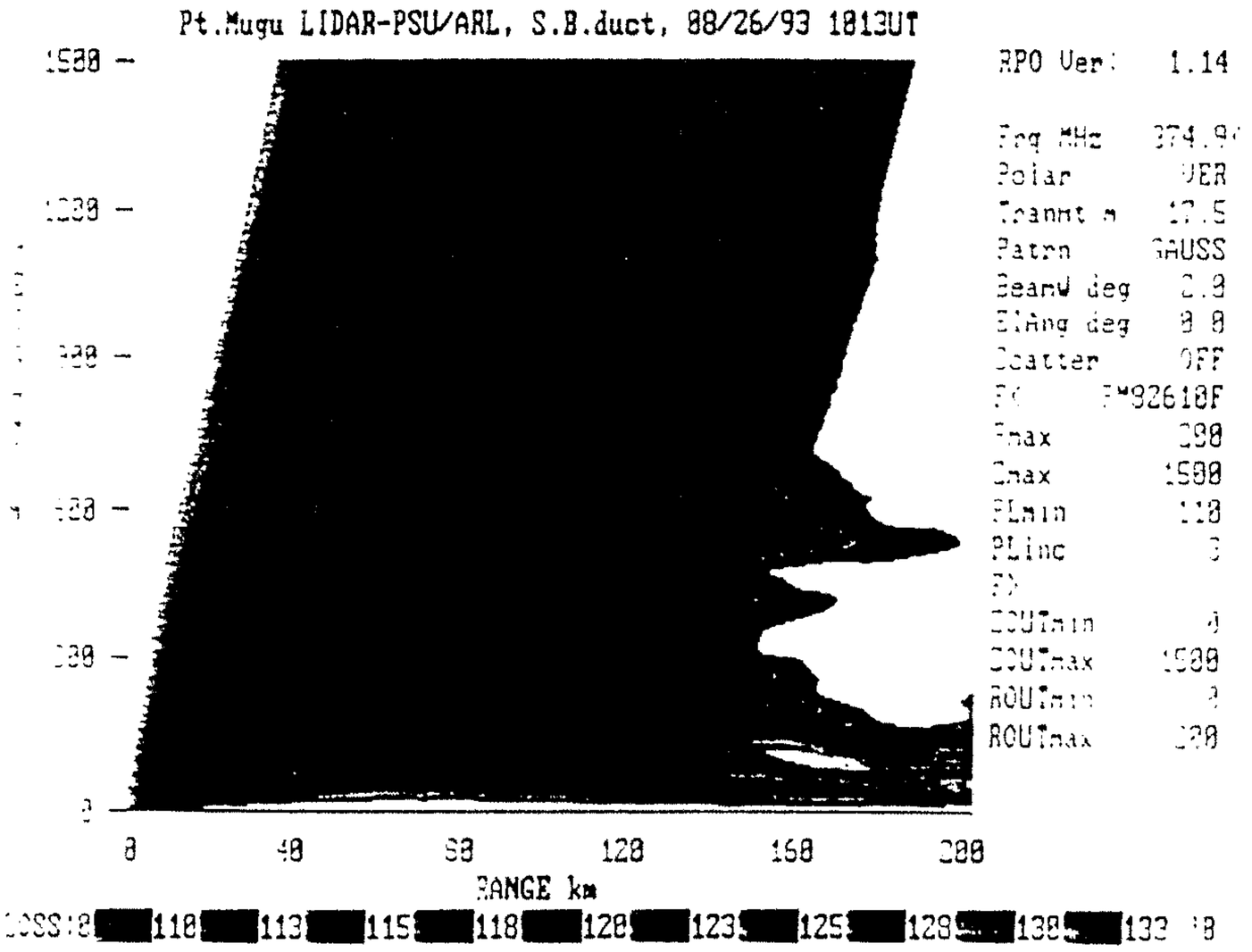

Figure 25. Propagation loss coverage output from RPO for UHF using the lidar result at 1013 UT on 26 August 1993

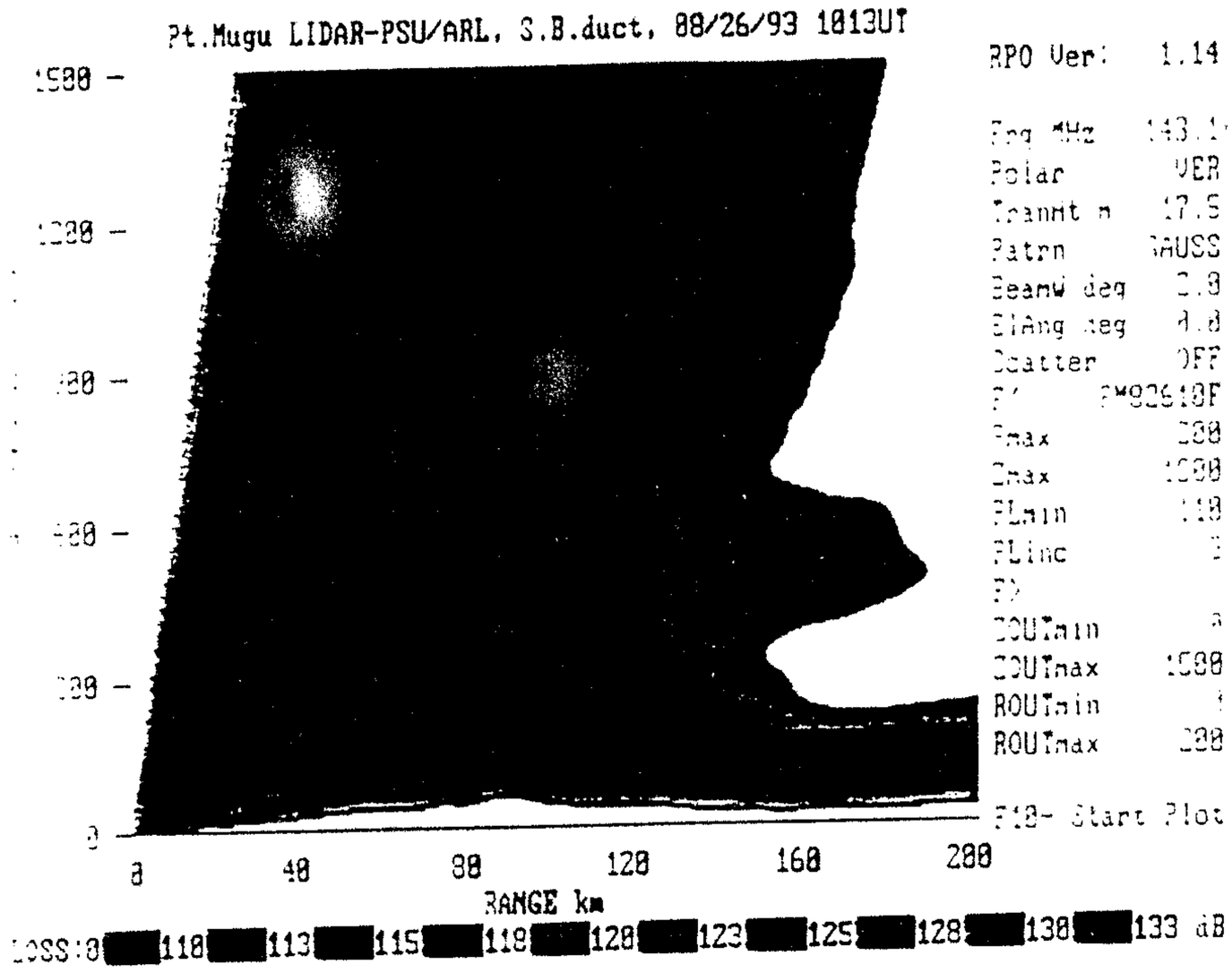

Figure 26. Propagation loss coverage output from RPO for VHF using the lidar result at 1013 UT on 26 August 1993.

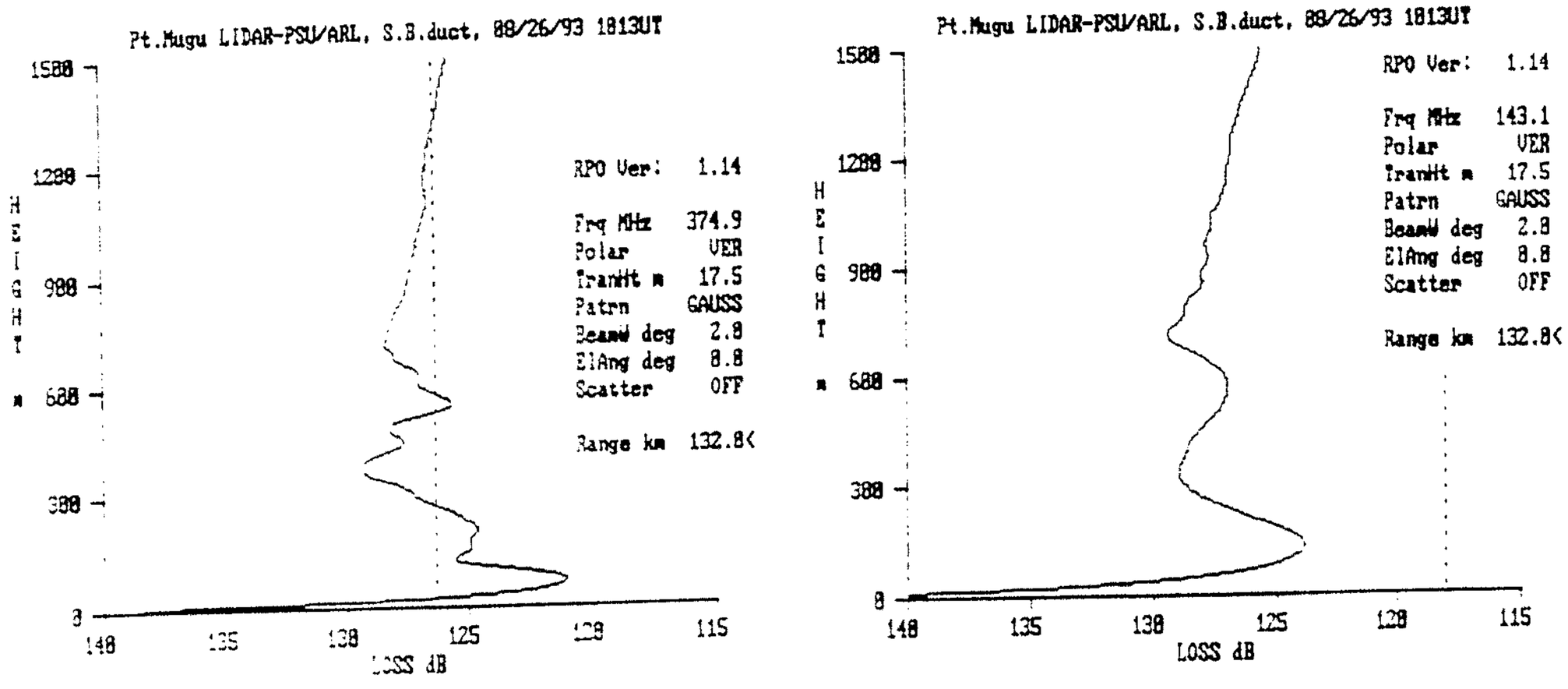

Figure 27. RPO model loss versus height showing enhanced signal at UHF (left) and VHF (right) compared to free space loss at 1013 on 26 August 1993

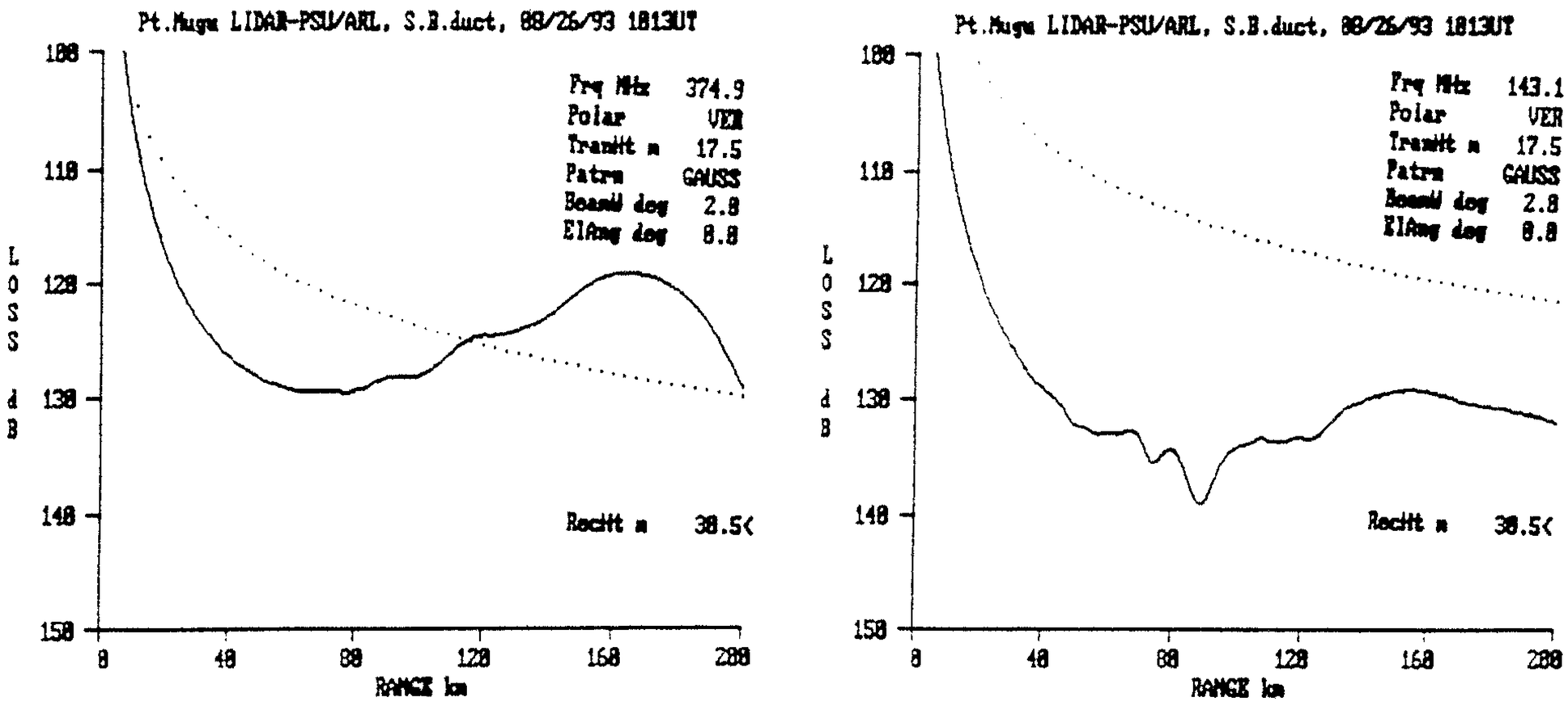

Figure 28. RPO model loss versus range at UHF (left) and VHF (right) compared to free space loss (dotted line) at 1013 on 26 August 1993.

ACKNOWLEDGEMENTS

The preparation of the LAMP instrument and these measurements have been supported by Oceanographer of the Navy through the Navy's Environmental Systems Program Office (SPAWAR PMW-165), the Naval Command Control and Ocean Surveillance Center (Code 54) and the National Science Foundation's CEDAR (Coupling Energetics and Dynamics of Atmospheric Regions) Program. The measurements on the RV *Polarstern* were made possible by invitation of the Alfred-Wegener-Institut which is gratefully acknowledged. Special appreciation for opportunity to directly tie the lidar derived refractivity to the measurements of electromagnetic wave ducting goes to J. Richter, H. Hitney, R. Paulus and T. Rogers of NRad. J. Rosenthal, J. Borgen and R. Helvey of the meteorological office of Geophysics Division and Safety Officer G. Wadley of the Naval Air Warfare Center at Point Mugu, CA contributed much to the success of the project. The efforts of D. B. Lysak, Jr., R. E. Erdley, T. J. Kane, J. Jenness, T. Petach, T. D. Stevens, P. A. T. Haris, Y.-C. Rau, S. Rajan, B. Mathason, M. O'Brien, S. C. McKinley, S. Maruvada, G. Evanisko, G. Pancoast, W. W. Moyer and E. Harpster have contributed much to the success of this project.

REFERENCES

Arshinov, Yu. F., S. M. Bobrovnikov, V. E. Zuev and V. M. Mitev, "Atmospheric temperature measurements using a pure rotational Raman lidar," Appl. Optics 22, 2984-2990, 1983.

Cooney, J. A., "Measurements on the Raman component of laser atmospheric backscatter," Appl. Phys. Lett., 12, 40-42, 1968.

Cooney, J. A., "Remote measurement of atmospheric water vapor profiles using the Raman component of laser backscatter," J. Appl. Meteor., 9, 182-184, 1970.

Cooney, J. A., "Comparisons of water vapor profiles obtained by rawinsonde and laser backscatter," J. Appl. Meteor., 10, 301-308, 1971.

Cooney, J. A., "Measurement of atmospheric temperature profiles using the Raman component of laser backscatter," J. Appl. Meteo. 11, 108-112, 1972.

Croskey, C. L., C. R. Philbrick, J. P. Martone, T. D. Stevens, P. A. T. Haris, J. J. Olivero, S. E. Puliafito and S. C. McKinley, "A Comparison of Microwave Radiometer, Lidar, and Meteorological Balloon Observations of Water Vapor During the LADIMAS Campaign," Proceedings of the IEEE Topical Symposium on Combined Optical-Microwave Earth and Atmosphere Sensing, 203-206, 1993.

Grant, W. B., "Differential absorption and Raman lidar for water vapor profile measurements: a review," Optical Engineering, 30, 40-48, 1991.

Haris, P. A. T., T. D. Stevens, S. Maruvada and C. R. Philbrick," Latitude Variation of Middle Atmosphere Temperatures," Advances in Space Research, 13, (9)83-87, 1994.

Hauchecorne, A., M. L. Chanin, P. Keckhut, and D. Nedeljkovic, "Lidar monitoring of the temperature in the middle and lower atmosphere," Appl. Phys. B55, 29-34, 1992.

Helvey, R., J. Rosenthal, C. R. Philbrick, T. J. Kane and D. B. Lysak, Jr., "LIDAR and Radiosonde Measurements of Coastal Atmospheric Refraction." Proceeding of the SPIE Symposium on Atmospheric Propagation and Remote Sensing III, Volume 2222, 1994.

Hitney, H. V., J. H. Richter, R A. Pappert, K. D. Anderson, and G. B. Baumgartner, Jr. "Tropospheric Radio Propagation Assessment," Proc. IEEE, Vol. 73, No. 2, Feb. 1985, pp. 265-283.

Hitney, H. V., "Engineer's Refractive Effects Prediction System (EREPS)," NATO/AGARD Conf. Proc., Operational Aids for Exploiting or Mitigating EM Propagation Effects," AGARD-CP-453, 15-19 May 1989 Symp., Sept. 1989, pp. 6-1 to 6-10.

Inaba, H., and T. Kobayasi, "Laser-Raman Radar," Opto-electronics, 4, 101-123, 1972.

Leonard, D. A., "Observation of Raman scattering from the atmosphere using a pulsed nitrogen ultraviolet laser," Nature 216, 142-143, 1967.

Melfi, S. H., J. D. Lawrence Jr. and M. P. McCormick, "Observation of Raman scattering by water vapor in the atmosphere," Appl. Phys. Lett., 15, 295-297, 1969.

Melfi, S. H., D. Whiteman and R. Ferrare, "Observations of atmospheric fronts using Raman lidar moisture measurements," J. Appl. Meteo., 28, 789-806, 1989.

Maruvada, S., Y.-C. Rau, G. R. Evanisko and C. R. Philbrick, "Laser Scattering in Clouds," Proceedings of the IEEE Topical Symposium on Combined Optical-Microwave Earth and Atmosphere Sensing, 215-219, 1993.

McKinley, S. C. and C. R. Philbrick, "Tropospheric Water Vapor Concentrations Measured by a Penn State/ARL Lidar," Proceedings of the IEEE Topical Symposium on Combined Optical-Microwave Earth and Atmosphere Sensing, 185-188, 1993.

Nedeljkovic, D., A. Hauchecorne and M. L. Chanin, "Rotational Raman lidar to measure the temperature from the ground to 30 km," IEEE Trans. Geos. Remote Sens. 31, 90-101, 1993.

Paulus, R. A: "The Lorentz Reciprocity Theorem and Range-Dependent Propagation Modeling," IEEE Trans. Ant. & Prop., 42, No. 2, pp. 270-273, 1994.

Philbrick, C. R., D. B. Lysak, T. D. Stevens, P. A. T. Haris and Y.-C. Rau, "Atmospheric Measurements Using the LAMP Lidar during the LADIMAS Campaign," 16th International Laser Radar Conference, NASA Publication 3158, 651-654, 1992.

Philbrick, C. R., D. B. Lysak and Y.-C. Rau, "Lidar Measurements of Aerosol Scattering in the Troposphere and Stratosphere" Proceedings of the IEEE Topical Symposium on Combined Optical-Microwave Earth and Atmosphere Sensing, 107-110, 1993.

Philbrick, C. R., D. B. Lysak, T. D. Stevens, P. A. T. Haris and Y.-C. Rau, "Lidar measurements of middle and lower atmosphere properties during the LADIMAS campaign," Proceedings of the 11th ESA Symposium, ESA-SP-355, 223-228, 1994.

Philbrick, C. R., "Raman Lidar Measurements of Atmospheric Properties," Proceeding of the SPIE Symposium on Atmospheric Propagation and Remote Sensing III, Volume 2222, 922-931, 1994.

Rau, Y.-C., "Multi-wavelength Raman-Rayleigh lidar for atmospheric remote sensing," PhD dissertation, Penn State University, 1994.

Renaut, D. and R. Capitini, "Boundary-layer water vapor probing with a solar-blind Raman lidar: validations, meteorological observations and prospects," J. Atmos. Oceanic Tech., 5, 585-601, 1988.

Stevens, T. D., S. Maruvada, T. J. Kane and C. R. Philbrick, "Lidar Observations of Mt. Pinatubo Aerosols: Effects on the Global Radiation Budget," Proceedings of the OSA Sixth Topical Meeting on Optical Remote Sensing of the Atmosphere, 5, 313-316, 1993.

Stevens, T. D., P. A. Haris, Y.-C. Rau and C. R. Philbrick, "Latitudinal Lidar Mapping of Stratospheric Particle Layers," Advances in Space Research, 13, (9)193-198, 1994.

Strauch, R. G., V. E. Derr and R. E. Cupp, "Atmospheric water vapor measurement by Raman lidar," Remote Sens. Envir. 2, 101-108, 1972.

Vaughan, G., D. P. Wareing, L. Thomas and V. Mitev, "Humidity measurements in the free troposphere using Raman backscatter," Q. J. R. Meteorol. Soc., 114, 1471-1484, 1988.

Whiteman, D. N., S. H. Melfi and R. A. Ferrare, "Raman lidar system for the measurement of water vapor and aerosols in the Earth's atmosphere," Appl. Optics 31, 3068-3082, 1992.